Broad Neutralization of Ebolaviruses via a Fusion Loop Epitope Elicited by Immunization

Xuelian Zhao[1#], Katie A. Howell[2#], Shihua He[3,4], Jennifer M. Brannan[5], Anna Z. Wec[6], Edgar Davidson[7], Hannah L. Turner[8], Chi-I Chiang[1], Lin Lei[1], J. Maximilian Fels[6], Hong Vu[2], Sergey Shulenin[2], Ashley N. Turonis[2], Ana I. Kuehne[5], Guodong Liu[3,4], Mi Ta[7], Yimeng Wang[1], Christopher Sundling[9], Jennifer S. Spence[6], Benjamin J. Doranz[7], Frederick W. Holtsberg[2], Andrew B. Ward[8], Kartik Chandran[6], John M. Dye[5], Xiangguo Qiu[3,4], Yuxing Li[1*], M. Javad Aman[2*]

[1]Institute for Bioscience and Biotechnology Research, University of Maryland, Rockville, MD 20878, USA; [2]Integrated BioTherapeutics, Inc., Rockville, MD 20850, USA; [3]Special Pathogens Program, National Microbiology Laboratory, Public Health Agency of Canada, Winnipeg, MB R3E 3R2 Canada and [4]Deparment of Medical Microbiology, University of Manitoba, MB R3E 0J9, Canada; [5]US Army Medical Research Institute of Infectious Diseases, Frederick, MD, USA; [6]Department of Microbiology and Immunology, Albert Einstein College of Medicine, Bronx, NY, USA; [7]Integral Molecular, Philadelphia, PA 19104, USA; [8]Department of Integrative Structural and Computational Biology, The Scripps Research Institute, La Jolla, CA 92037, USA; [9] Immunology division, Garvan Institute of Medical Research, Darlinghurst, New South Wales 2010, Australia

# These authors contributed equally to this work

*Correspondence authors: M. Javad Aman, javad@integratedbiotherapeutics.com;

Yuxing Li, liy@ibbr.umd.edu

Integrated BioTherapeutics, Inc.

4 Research Ct., Suite 300

Rockville, MD 20850

Abstract

While neutralizing antibodies are highly effective against ebolavirus infections, current experimental ebolavirus vaccines primarily elicit species-specific antibody responses. Here we describe an immunization-elicited macaque antibody (CA45) that clamps the internal fusion loop with the N-terminus of the ebolavirus glycoproteins (GP) and potently neutralizes Ebola, Sudan, Bundibugyo, and Reston viruses. CA45, alone or in combination with an antibody that blocks receptor binding, provided full protection against all pathogenic ebolaviruses in mice, guinea pigs, and ferrets. Analysis of memory B cells from the immunized macaque suggests that elicitation of broadly neutralizing antibodies (bNAbs) for ebolaviruses is possible but difficult, potentially due to the rarity of bNAb clones and their precursors. Unexpectedly, germline-reverted CA45, while exhibiting negligible binding to full-length GP, bound a proteolytically remodeled GP with picomolar affinity, suggesting that engineered ebolavirus vaccines could trigger rare bNAb precursors more robustly. These findings have important implications for developing pan-ebolavirus vaccine and immunotherapeutic cocktails.

Introduction

Members of the family *Filoviridae* (filoviruses) are among the viruses with the highest mortality and no approved treatments or vaccines available for human use. There are five known ebolavirus species: Ebola (EBOV), Sudan (SUDV), Bundibugyo (BDBV), Reston (RESTV), and Taï Forest (TAFV) viruses, a cuevavirus, as well as two marburgviruses: Marburg virus (MARV) and Ravn virus (RAVV) (Kuhn et al., 2014). Since 1967 multiple outbreaks of MARV, SUDV, and BDBV have been recorded and in the recent Ebola virus disease epidemic in 2014, caused by the Zaire EBOV, the virus seems to have mutated to infect humans more efficiently (Diehl et al., 2016). Current vaccines and immunotherapeutics advancing through late stage development are specific for EBOV (Zaire). Given the unpredictable nature of future outbreaks and viral resistance, broadly protective vaccines and antibody therapeutics for filoviruses are critically needed.

Filovirus entry is mediated by the trimeric filovirus glycoproteins (GP), which consist of disulfide-linked GP1 and GP2 subunits, with GP1 forming a chalice like structure wrapped around by GP2 (Lee et al., 2008; Zhao et al., 2016). GP2 and an N-terminal portion of GP1 form the base of the chalice. GP1 contains the receptor binding site (RBS) positioned on the trimer apex and is largely concealed by a glycan cap and a highly glycosylated and disordered mucin-like domain (MLD). Filoviruses enter endosomes via micropinocytosis, and are trafficked to late endosomal compartments, where the cysteine proteases cathepsin B and L cleave off the MLD and the glycan cap, leading to the exposure of the RBS and allowing GP1 to interact with its endosomal receptor Niemann Pick C1 (NPC1) (Bornholdt, 2016; Miller et al., 2012; Wang et al., 2016a). Upon binding to the luminal domain C of NPC1, and in response to an undefined trigger, GP2 is proposed to undergo substantial rearrangements that allow insertion of the internal fusion loop (IFL) into the endosomal membrane and initiate membrane fusion through the formation of a six-helix bundle (Lee and Saphire, 2009).

Three mechanisms of neutralization have been postulated for ebolaviruses: inhibition of cathepsin-mediated cleavage, blockade of NPC1 binding, and mechanical interference with the structural rearrangements of GP2 required for fusion (Saphire and Aman, 2016).The best characterized neutralizing epitope within EBOV GP is the 'base epitope', consisting of residues at the GP1/GP2 interface, which is recognized by the monoclonal antibody (mAb) KZ52 (Davidson et al., 2015; Lee et al., 2008) and, with a slightly different angle, by two ZMapp™ components c2G4 and c4G7 (Davidson et al., 2015; Murin et al., 2014; Tran et al., 2016). While these base binders are potent neutralizers, they are species-specific and only neutralize EBOV. A similar base-binder, 16F6, was also reported to neutralize SUDV only (Dias et al., 2011). Recently, we and others have identified several novel cross-neutralizing epitopes within the RBS (Howell et al., 2016; Keck et al., 2015) and the glycan cap (Bornholdt et al., 2016; Flyak et al., 2016; Holtsberg et al., 2015), and GP2 suggesting that development of broadly neutralizing therapeutic antibodies (bNAbs) and cross protective vaccines may be feasible.

Here we report an ebolavirus bNAb (CA45) elicited by immunization of cynomolgus macaques that binds to a conserved epitope positioned within the IFL that partially overlaps with those of base binders, KZ52, c2G4, and c4G7. CA45 potently neutralizes EBOV, SUDV, and BDBV, the only ebolaviruses known to cause lethal disease in humans, and protects rodents from EBOV and SUDV infection. Furthermore, a cocktail of the IFL-binding mAb CA45 with the RBS-binding mAb FVM04 fully protects guinea pigs from lethal infection in a synergistic manner and provides full protection against BDBV infection in ferrets. This mAb combination represents a promising candidate as pan-ebolavirus therapeutic. Furthermore, this study has important implications for vaccine development. Unexpectedly, we found that a proteolytically remodeled GP resembling the endosomal form of GP (cathepsin cleaved) binds with $>10^6$ fold higher affinity to the CA45 germline precursor compared to full length GP, indicating that similar modification of vaccine candidates could potentially enhance the elicitation of CA45-like bNAbs.

The isolation of bNAbs against ebolavirus from vaccinated nonhuman primates (NHPs), their superior protective efficacy as mono- or combination therapy, and the prospect of germline targeting by vaccine re-design strongly support the premise of pan-ebolavirus therapeutic cocktails for therapy and a pan-ebolavirus vaccine for prevention.

Results

Isolation of ebolavirus cross-reactive mAbs

In this study, we aimed to analyze the vaccine-elicited cross-reactive B cell response to the GPs of ebolaviruses in IgG-switched memory B cells from a previously immunized cynomolgus macaque (NHP #20667) (Keck et al., 2015). The macaque was immunized 3 times with a trivalent filovirus GP cocktail consisting of EBOV/SUDV/MARV GPΔmuc (ectodomain lacking MLD) (Keck et al., 2015). The serum of NHP #20667 demonstrated neutralization capacity against EBOV, SUDV, and BDBV (Figure 1A), suggesting that ebolavirus cross-reactive B cells may exist in this animal. We sought to clone these cross-reactive mAbs from the peripheral B cells using multicolor antigen-specific memory B cell fluorescence-activated cell sorting (FACS) and Ig cloning method that has been established and optimized recently for NHP B cell repertoire analysis (Sundling et al., 2012; Wang et al., 2016b). Using a fluorescently labeled memory B cell surface marker cocktail along with GPΔmuc of EBOV and SUDV, we stained the peripheral blood mononuclear cells (PBMCs) isolated 4 weeks after the third immunization and sorted out cross-reactive surface IgG^+ memory B cells. GP cross-reactive memory B cells ($CD20^+IgG^+$Aqua $blue^-CD14^-CD3^-CD8^-CD27^+IgM^-$, EBOV $GP\Delta muc^{hi}$ SUDV $GP\Delta muc^{hi}$) (Figure 1B) were sorted at single cell density into individual wells of micro-titer plates, followed by RT-PCR amplification of the Ig heavy- and light-chains.

Within the memory B cell compartment of this macaque, about 0.5% of the cells were GP-specific (Table S1), with the frequency of cross-reactive GP-specific memory B cells being 0.06%, accounting for ~10% of GP-specific memory B cells (Table S1). From ~$6x10^6$ PBMCs, we sorted 28 ebolavirus family GP cross-reactive memory B cells. Paired heavy/light chains (HC/LC) were obtained for 17 cells. Of these,12 clones were expressed as full length IgG1 for ELISA assay (Table S1). Over 90% of the clones (11/12) were found to bind both EBOV and SUDV GPΔmuc (Figure 1C), validating the sorting method. Analysis of the HC and LC variable

regions (V_H and V_L) along with the HC/LC complementarity determining region 3 (CDRH3 and CDRL3) revealed that 4 of 11 clones were related to each other and/or to clones identified by yeast display method in our previous study (Keck et al., 2015), while the remaining 7 were single member clones (Table S2), suggesting a diverse cross-reactive GP-specific B cell repertoire. In a neutralization assay with recombinant vesicular stomatitis virus (rVSV) pseudotyped with either EBOV or SUDV GP, we found that ~60% (6/11) of the isolated antibodies were non-neutralizing, while ~30% (4/11) were found to neutralize rVSV with either EBOV or SDUV GP (Table S2). Only one clone, , CA45, neutralized both EBOV and SUDV (Table S2), and was selected for further analysis as a bNAb.

Binding and functional characterization of bNAb CA45

Since filovirus receptor interactions and cellular membrane fusion occur in the acidic environment of endosomes, we examined CA45 binding to GP ectodomains (GPΔTM) of EBOV, SUDV, BDBV, and RESTV at both acidic and neutral pH by ELISA. CA45 strongly bound to GPΔTM of EBOV, SUDV, BDBV, and to a lesser extent to RESTV at both acidic and neutral pH (Figure 2A). The strongest binding was observed for BDBV with EC_{50} values ranging from 0.21 to 0.34 nM at different pH (Figure 2A) and the weakest binding for RESTV with EC_{50} values of 20-50 nM. For all four viruses, the reactivity of CA45 was moderately enhanced at acidic pH.

In the endosomes, filovirus GP is cleaved by cysteine cathepsins to yield a 19 kDa truncated GP1 fragment associated with GP2 (cleaved GP; GP_{CL}) in which the RBS is exposed (Chandran et al., 2005). GP_{CL} interacts with NPC1 and mediates the fusion of viral and endosomal membranes (Carette et al., 2011). As shown in Figure 2A, CA45 bound to GP_{CL}, about 23, 14, and 7-fold better than to GPΔTM at pH7.5, 5.5, and 4.5, respectively. In contrast, no binding was observed to soluble GP (sGP), the product of the unedited EBOV GP gene (residues 1-295 followed by a unique C-terminal tail) (Figure 2A). These data indicate that

CA45 binding does not require the MLD or the glycan cap and that removal of these domains reduces the constraints on CA45 binding.

Biolayer interferometry (BLI) was used to evaluate the kinetics of CA45 binding to EBOV, SUDV, BDBV, RESTV GPΔTM and EBOV GP_{CL} (Figure 2B). The association and dissociations of the mAb+GP complexes fit a 1:1 binding model. The K_D values for GPΔTM were determined to be approximately 10.6 nM for EBOV, 3.3 nM for SUDV, 1.2 nM for BDBV, and 161 nM for RESTV, respectively. Consistent with the ELISA data, CA45 bound EBOV GP_{CL} with higher affinity (sub picomolar) than EBOV GPΔTM.

We then tested the ability of CA45 to neutralize a replication competent rVSV pseudotyped with filovirus GP, which also expressed the reporter protein GFP (rVSV-GP-GFP) (Miller et al., 2012). CA45 potently neutralized rVSV pseudotyped with EBOV, SUDV, BDBV, and to a lesser extent RESTV, but not TAFV and LLOV (Figure 2C). To confirm that the neutralization is due to inhibition of cellular entry, CA45 was tested in a single round infection assay using a VSV-GP pseudovirus expressing luciferase (rVSV-Luc) (Howell et al., 2016). CA45 potently cross-neutralized EBOV, SUDV, and BDBV pseudotypes in this assay indicating that it functions by inhibiting cellular entry. To examine if CA45 could neutralize the cathepsin-primed form of EBOV that mediates membrane fusion, we treated rVSV-GP viruses with thermolysin to generate particles displaying GP_{CL}. Interestingly, the neutralizing potency of CA45 towards rVSV expressing GP_{CL} of EBOV, SUDV, and BDBV was dramatically higher (100-, 1900-, and 600-fold reduction of IC_{50}, respectively) compared to full length GP (Figure 2C). This is consistent with the strikingly higher binding affinity of CA45 to GP_{CL} compared to GPΔTM. In contrast, KZ52 did not show any neutralizing activity towards cleaved EBOV (Figure 2C). The broadly neutralizing activity of CA45 was also confirmed in plaque reduction neutralization tests (PRNT) using the authentic ebolaviruses (Figure 2C).

The contrast between CA45 and KZ52 in neutralization capacity against EBOV bearing cleaved GPs (GP_{CL}) suggested that KZ52 may be acting upstream of cathepsin cleavage and CA45 downstream. We therefore performed a series of experiments to elucidate the step(s) of entry affected by CA45 and KZ52. As expected neither CA45 nor KZ52 had any effect on the binding of GP_{CL} to NPC1 (Figure S1A). We then examined the effect of CA45 and the base-binder KZ52, as well as the EBOV mAb100 (Misasi et al., 2016) on cathepsin L cleavage of GP, in a Western blot of GP cleavage product by cathepsin L in the presence of antibodies (Figure S1B). CA45 showed partial inhibition of cathepsin cleavage evident by the accumulation of partially cleaved GP species and the weaker band of completely cleaved GP (GP_{CL}) compared to the control antibody, while mAb100 exhibited nearly complete inhibition (Figure S1B). The base binder KZ 52 displayed moderate inhibitory effect on GP cleavage (Figure S1B). Using a live cell imaging assay (Spence et al., 2016), we further evaluated if CA45 blocks fusion triggering, an early stage of virus-cell membrane fusion. As shown in Figure S1C, viral fusion triggering, as indicated by membrane lipid mixing, was not significantly inhibited by CA45, contrasting to KZ52. Furthermore, no significant difference in co-localization of internalized virus particles with NPC1 was observed following incubation of virus and cells with CA45, indicating that CA45 does not affect receptor binding. Collectively, these data suggest that CA45 may be acting at two stages of virus entry; 1) by inhibiting cathepsin cleavage, and 2) inhibition at a late stage when the productive fusion between the viral and the endosomal membrane occurs.

Scanning mutagenesis of CA45 suggests a primary role for heavy chain in GP binding

Analysis of the VH and VL regions of CA45 revealed that the closest inferred cynomolgus macaque germline precursor was IGHV4-21 and IGKV1-5, respectively (Figure 3A). CA45 had a moderate level of somatic hypermutation (SHM, 9.9% nt and 14% aa for VH, and 7.5% nt and 14% aa for Vκ, respectively) and a 19-aa CDRH3 loop (Figure 3A) (Table S3).

It is of note that there is one amino acid deletion in CDRH1 and that the CDRH3 is flanked by two negatively charged residues D95 and D101 and contains eight highly hydrophobic residues (F,I,V,W, and L) (Figure 3A), which may relate to important molecular recognition function.

To examine the molecular basis and the role of CDR residues in CA45-GP interaction, we performed alanine-scanning mutagenesis of CA45 CDRs and investigated the effect of each substitution on CA45 binding to EBOV (Figure 3B), SUDV and BDBV GPs (Figure 3C and Figure S2). Interestingly, only mutations in CDRH1 and CDRH3 caused dramatic decrease of CA45 binding to GP, while substitutions in CDRH2 and all the LC CDRs had little impact (Figure 3B, C, and Figure S2). This implies that the heavy chain of CA45 has a major role in GP-recognition and that the light chain may play a minor role. Most of the residues in CDRH1 and CDRH3 that are critical for CA45-GP binding are either highly hydrophobic (Y32, Y33, W35, F98, I100, F100a, I100e, W100h) or negatively charged (D95 and D101) (Figure 3C), suggesting that hydrophobic interactions and salt-bridges may be heavily involved in the CA45-GP recognition interface.

To analyze the importance of SHM for CA45, we reverted both the heavy- and light-chain sequences to that of the naïve B cell precursor inferred from the germline IGHV4-21 and IGKV1-5, respectively (Figure 3A), and produced the germline reverted CA45 (CA45-$H_{GL}L_{GL}$) for functional analysis. CA45-$H_{GL}L_{GL}$ showed very weak binding for GPΔmuc of EBOV and SUDV and no binding to GPΔTM of BDBV (Figure 3D and Figure S3). Unexpectedly, CA45-$H_{GL}L_{GL}$ exhibited sub-picomolar affinity to GP_{CL}, indistinguishable from the mature CA45. These data suggest that steric constraints of GP molecules limit the ability of the CA45 germline precursor to access its cognate epitope on GP, which can be eased by the removal of the MLD and glycan cap. Consistent with our observation that CA45 HC plays a major role in GP recognition, CA45-H_mL_{GL}, a semi-reverted CA45 containing mature heavy chain and germline light chain, bound EBOV GPΔmuc with similar affinity as mature CA45 (6.9 nM for CA45-H_mL_{GL} vs. 3.2 nM for

CA45, Figure 3D). However, CA45-H_mL_{GL} exhibited 12-fold and 35-fold poorer affinity to GPs of SUDV and BDBV, respectively (Figure 3D). The reverted antibodies were also tested in neutralization assays. As expected against wild type GP, no neutralization was observed with CA45-$H_{GL}L_{GL}$, while the semi-reverted CA45-H_mL_{GL}, showed detectable but severely reduced neutralizing potency against all three viruses (Figure S3), indicating that the light chain maturation of CA45 is important for effective neutralization.

Epitope mapping of CA45

To determine the GP epitope surface recognized by CA45, we evaluated the competition between CA45 and a series of EBOV mAbs with known epitopes using BLI. CA45 did not compete with the glycan cap binder 13C6, RBS binder FVM04, or with FVM02 which binds to the tip of the IFL (Table S4). However, CA45 strongly competed with KZ52 (Table S4), suggesting that their epitopes are closely positioned, perhaps at the GP base.

To identify the critical GP residues required for CA45 binding, we used an alanine scanning approach, where the binding of CA45 and two control mAbs was evaluated against a 'shotgun mutagenesis' Ala-scan library of EBOV GP in which 641 of 644 GP residues were individually mutated. HEK-293T cells were transfected with the entire library in a 384-well array format and assessed for reactivity to CA45 by high-throughput flow cytometry (Figure 4A). Two other GP antibodies, FVM04 and FVM09 (Keck et al., 2015), were included as controls for proper protein folding and expression. The epitope mapping identified EBOV GP residues R64 within the N-terminus of GP1 in addition to Y517, G546, and N550 within the IFL of GP2 as critical for CA45 binding (Figure 4A, B). Compared to wild type GP, alanine substitutions at these residues reduced CA45 binding by 98%, 96%, 89%, and 78%, respectively, while the binding of FVM04 and FVM09 to these mutants was not reduced (Figure 4B).

All four of these residues are highly conserved among GPs of all ebolaviruses (Figure 4C). R64 is located within the β3 strand at the N-terminus of EBOV GP1 and is identical

between Kikwit, Mayinga, and Makona strains of EBOV, while SUDV, BDBV, TAFV, and RESTV have a lysine residue with similar charge as arginine at this position. Y517 and G546 are positioned in strands β19 and β20 within the IFL and are identical among all ebolavirus species (Figure 4C). N550, located in the β20-α3 (HR1-A) loop, is also conserved among all filoviruses and is shared by the KZ52 epitope (Davidson et al., 2015). In contrast, except for the residues within β20 and β20-α3 loop, marburgvirus GP shows little homology in this region (Figure 4C), consistent with the lack of CA45 binding to marburgvirus GPs (not shown). The key residues are clustered closely within the base of the GP trimer structure (Figure 4D). In addition to these four mutations that reduced CA45 binding to GP by >75%, alanine substitution of neighboring residue K190 (Figure 4D) also reduced CA45 binding by 67% without affecting control antibody binding, suggesting that K190 may also be important for CA45 binding to GP.

The key CA45 contact sites largely overlap in the overlay of GPΔmuc (5JQ3) and GP_{CL} (5HJ3) structures (Figure S4A), suggesting that the dramatically increased affinity of CA45 and CA45-$H_{GL}L_{GL}$ for GP_{CL} compared to GPΔmuc does not relate to changes in the configuration of these residues upon cleavage. However, in GPΔmuc the bulky residues D192, F193, and F194 are positioned in the middle of the CA45 epitope, while in GP_{CL} these residues are disordered (Figure S4A). These same residues, referred to as the "DFF lid", were reported to block access to the binding pocket for toremifene, a small molecule inhibitor of EBOV membrane fusion (Zhao et al., 2016) (Figure S4B). Interestingly, alanine substitution of D192, F193, and F194 increased CA45 binding to 170%, 182%, and 224% of wild type GP, respectively (Figure S4C), suggesting that the "DFF lid" interferes with CA45 binding to GP. Displacement of the DFF lid in GP_{CL} may allow CA45 and its germline precursor to better access the cognate epitope.

We further sought to delineate which GP residues possibly permit escape from antibody binding and neutralization by isolating CA45 escape mutants using the recombinant VSV-EBOV GP pseudotype system. The virus was grown in Vero cells in the presence of increasing

concentrations of CA45 for four passages and the resulting virus population was plaque purified, and individual clones were sequenced. All of the isolated escape clones contained the two mutations A101V and K588R with two variants harboring a third mutation of either N643D or A654T in the membrane proximal extracellular region of GP (Figure S5A&B). These mutants showed strongly reduced binding to CA45 (Figure S5C) and, as expected, could not be neutralized by CA45 (Figure S5D). Interestingly, none of the CA45 contact residues identified by alanine scan mutagenesis were found mutated among escape variant GPs, suggesting that mutations of these residues may be detrimental for viral fitness. Neither A101 nor K588 is exposed on the GP surface, while the orientation of N643 and A654 are unknown as they are not included in the existing crystal structures of GP. The combined mutations likely have a structural impact on the CA45 binding site. In our GP alanine scanning study, the single mutants of A101S, K588A, N643A, or A654S did not show any significant change in binding to CA45 (Figure S5E), suggesting that only combinations of these mutations can lead to escape by altering the epitope environment (Figure S5B), as both A101 and K588 are in proximity of the GP residues R64 and Y517 that are critical for CA45 binding (Figure S5B). As expected, the CA45 escape mutants were readily neutralized by the RBS binding mAb FVM04 (Figure S5F).

Electron Microscopy reconstruction

In order to better understand how CA45 interacts with GP, we derived a 3D negative stain EM reconstruction of the CA45 Fab bound to EBOV GPΔTM (Figure 5A and Figure S6). CA45 approaches GP with a nearly perpendicular angle and binds the GP region proximal to the internal fusion loop (IFL), (Figure 5B). As suggested by the scanning mutagenesis data of CA45 (Figure 3C), the CDRH1 and CDRH3 of CA45 that play a major role in GP recognition most likely bind to GP residues proximal to the IFL. A homology model of CA45 was docked to orient the heavy chain and revealed that the CDRH1 and CDRH3 variable loops interact closely with the GP residues surrounding the IFL (Figure 5C). In this CA45-GP model, residues R64,

Y517, G546 and N550 on GP (Figure 5C, shown in dark blue) that are important for CA45 binding, face toward the CA45 CDRs, consistent with the GP alanine scanning data. Residue K190 on GP (Figure 5C) also has an effect on CA45 binding when mutated to alanine, but may not be as critical as these other four residues.

Consistent with the binding competition analysis, the EM data showed that KZ52 Fab binds to an epitope that overlaps with that of CA45, however at a different angle and targets some non-conserved GP residues (Figure 5D). Conversely, CA45 binds to a more conserved region of filovirus GP, which likely confers its cross-reactivity (Figure 5D). Thus, our data reveals the molecular basis for the neutralization breadth of CA45, which in comparison with related, but EBOV strain-specific, neutralizing antibodies, including KZ52 and the ZMapp components, c2G4 and c4G7, target the proximal GP surface (Figure 5E).

In vivo protection against EBOV and SUDV in mice and guinea pigs

Post-exposure *in vivo* efficacy of CA45 was first tested in mouse models of EBOV and SUDV. Groups of 10 BALB/c mice were infected with 100 pfu of mouse-adapted EBOV (MA-EBOV) (Bray et al., 1999) followed by intraperitoneal (IP) injection of CA45 at doses ranging from 10 to 0.5 mg/kg (200 to 10 μg/mouse) or PBS as control, two days post infection (dpi). Highly significant protection from lethality was observed at all dose levels of CA45 compared to PBS-treated group, with $p<0.0001$ for doses above 1 mg/kg and $p=0.0119$ for 0.5 mg/kg (Figure 6A). Additionally, animals receiving CA45 showed less weight loss compared to controls, with only minimal weight loss evident at the highest dose of CA45 (10 mg/kg) (Figure 6A).

We then tested the efficacy of CA45 in a SUDV model using mice deficient for the IFNα receptor (B6.129S2-Ifnar1tm1Agt/Mmjax) (Brannan et al., 2015). In multiple experiments, mice were challenged with 1000 pfu of wild type SUDV and treated by a single IP injection of mAbs at 1 dpi. A dose of 10 mg/kg of CA45 protected 5 out of 6 animals from lethal infection and these mice exhibited an average of <6% weight loss compared to 28% in the PBS group (Figure 6B,

upper panel). We previously demonstrated partial protection against SUDV in this model using the RBS binding mAb FVM04 that blocks GP interaction with NPC1 (Howell et al., 2016). Here we hypothesized that combining a receptor blocker with a potential inhibitor of fusion may yield greater efficacy. To this end, we combined FVM04 and CA45 at 5 mg/kg each (Figure 6B upper panel) or 5 mg/kg of FVM04 plus 2.5 mg/kg of CA45 (Figure 6B, lower panel). Both combinations provided 100% protection against SUDV in independent experiments. Although survival curves between the groups treated with cocktail versus monotherapy were not significantly different, mice treated with the cocktail showed no weight loss (Figure 6B) or other signs of disease, unlike mice treated with single mAbs.

We also tested CA45 or FVM04 alone or in combination in a stringent guinea pig model of EBOV infection, in which a single dose of antibody was delivered at 3 dpi. Groups of 6 guinea pigs were infected with 1000 LD_{50} of guinea pig-adapted EBOV (GPA-EBOV) and treated 3 dpi with either FVM04 or CA45 at 5 mg/animal or a combination of the two mAbs at 2.5 or 5 mg each. Animals were treated with PBS as a negative control. Treatment with 5 mg of FVM04 or CA45 alone protected 1 out of 6 and 3 out of 6 animals, respectively (Figure 6C). PBS-treated animals died within 8 dpi (mean time to death: 7.5 days) and lost an average of 21% of body weight before succumbing to infection, while FVM04 or CA45 treated animals showed a mean survival time of 11.5 and 20.5 dpi and a maximum weight loss of 9.2% and 1.2%, respectively (Figure 6C). In contrast, all animals treated with a combination of either 2.5 or 5 mg of each mAb survived the infection with no sign of disease or weight loss (Figure 6C). The protection afforded by either monotherapy or combination therapy was significantly better compared to PBS treated guinea pigs (p=0.0018 and p<0.0001, respectively). Furthermore, combination therapy was significantly better than monotherapy for both CA45 (p=0.0079) and FVM04 (p <0.0001). These data, combined with the lack of weight loss in cocktail treated groups, indicate that combining the two mAbs strongly enhances the efficacy.

We have previously shown that FVM04 alone (5 mg) protects against SUDV infection in guinea pigs (Howell et al., 2016). Here we similarly evaluated if CA45 alone could also protect against SUDV in this model. As shown in Figure 6D, a single dose of 5 mg CA45 at 3 dpi protected all animals from lethal infection with GPA-SUDV, while all control guinea pigs died within 14 dpi (p<0.0001). CA45 treated animals also didn't show any weight loss upon SUDV infection, while controls lost up to 25% of their body weight (Figure 6D).

Protective efficacy in ferrets

Beside EBOV and SUDV, BDBV is the only other ebolavirus that has caused fatalities in humans. Although there are no rodent models for BDBV infection, a ferret model was recently developed that exhibits many features of filovirus disease in humans (Kozak et al., 2016). Since guinea pig protection data indicated that a combination of CA45 and FVM04 is optimal for effective control of EBOV infection, we sought to test this cocktail in the BDBV ferret model. A group of two male and two female ferrets, were infected with 253 $TCID_{50}$ of BDBV and treated at 3 and 6 dpi with 20 mg of each antibody by IP injection. A control group of 2 infected ferrets received PBS at the same time points. Control animals succumbed to infection 7 dpi while all four treated animals survived with no clinical signs of disease (Figure 7A, B). One animal (888M) experienced an unrelated accident on 21 dpi, which paralyzed both his hind legs. Because this animal was unable to reach food and water, he was euthanized on 22 dpi. Among the treated animals, the two male ferrets (808M and 888M) showed steady weight gain and no detectable virus in the blood, while the female animals (n=2) exhibited less weight gain and moderate viremia with ~10^4 GEQ/mL on day 6. Both control animals displayed very high viremia (~10^{10} GEQ/mL) (Figure 7 C&D). High viral load was also detected in oral, nasal, and rectal swabs of both control animals but none of the treated ferrets (Figure 7E-G).

Blood chemistry analysis showed a drastic rise in circulating levels of alkaline phosphatase, alanine aminotransferase, total bilirubin, blood urea nitrogen and potassium in

control animals (Figure 7H-L), similar to the disease course in humans and NHPs (Feldmann and Geisbert, 2011), while these parameters remained unaffected in treated animals (Figure 7H-L). Complete blood count (CBC) analysis showed a drop in white blood cell count, and a drastic reduction in total lymphocyte and platelet counts, which rapidly rebound only in treated animals (Figure S7). The complete results of the blood chemistry and CBC analysis is shown in Figure S7.

Discussion

In this study, we identified a novel bNAb, CA45 that targets a key site of vulnerability within the highly conserved ebolavirus IFL. CA45 neutralizes four out of five viruses of the genus Ebolavirus and displays *in vivo* protective efficacy in rodent and mustelid animal models of Ebola, Sudan and Bundibugyo viruses. CA45 exhibits unique features with respect to its pattern of reactivity to various forms of GP, properties of its germline precursor, as well as its conserved epitope that have important implications for design of effective pan-ebolavirus vaccines and therapeutics.

Importantly, CA45 was isolated from a vaccinated cynomolgus macaque, which display highly homologous Ig gene composition to humans, suggesting that bNAbs targeting conserved and highly vulnerable ebolavirus epitopes can be elicited by immunization in primates including humans. Analysis of the B cell compartment in this macaque indicated that memory B cells that encode bNAbs are of low frequency, accounting for 1% of the GP-specific and ~0.005% of total memory B cells. This observation is consistent with previous studies showing that the protective responses to prototypical ebolavirus vaccines are mostly strain specific (Mire et al., 2013). This may relate to low precursor frequency and/or inefficient activation of such precursors by the vaccine. Indeed, we observed very poor binding of the CA45 germline precursor (CA45-$H_{GL}L_{GL}$) to wild type GP. However, unexpectedly, CA45-$H_{GL}L_{GL}$ bound with high affinity to the endosomal form of GP (GP_{CL}) lacking MLD and the glycan cap. This may relate to better

accessibility of the cognate epitope in GP_{CL} and/or subtle conformational differences within the epitope in the full length versus cleaved form of GP that may impact the ability of the germline antibody to bind, consistent with the notion that these domains serve to conceal critical GP epitopes. It is likely that the GPΔMuc immunogen cocktail used in this study has contributed to our ability to elicit these rare B cell precursors. Recently, optimized HIV Env immunogens have been designed that, unlike wild type Env, effectively elicit precursors of HIV-1 bNAbs (Jardine et al., 2013; McGuire et al., 2016; Sok et al., 2016). The proteolytically remodeled GP_{CL} represents a germline-targeting immunogen that could potentially trigger CA45-like precursor B cells and lead to cross protective responses. Thus, future strategies aiming at efficiently expanding the bNAb memory B cell and/or plasmablast populations should focus on specific design of immunogens/immunization regimens that enhance the epitope exposure and elicitation of such rare precursors. Such modifications could include deletion of MLD, enzymatic or genetic removal of the glycan cap, and potentially further resurfacing by introducing additional mutations to enhance the immunogen binding to precursors for other bNAbs such as those binding to the RBS or the stalk.

The prototypic and the best characterized filovirus neutralizing epitope, the so-called “base epitope”, is targeted by EBOV-specific antibodies such as KZ52 (Lee et al., 2008), the ZMapp™ components c2G4 and c4G7 (Murin et al., 2014), as well as SUDV-specific mAbs 16F6 (Dias et al., 2011), E10, and F4 (Chen et al., 2014). This epitope consists of residues at the GP1/GP2 interface within the base of the trimeric GP with no cross-neutralizing mAbs targeting this epitope previously reported. CA45 strongly competes with KZ52 and c2G4 for GP binding and yet displays broad binding and neutralizing activity. Our epitope-mapping data indicate that CA45 targets the IFL and contacts residues in both GP1 and GP2 with a footprint that partially overlaps the “base epitope”, while approaching GP at a different angle compared to KZ52, tilted towards the tip of the IFL (Figures 4D &5D). The footprint of CA45 defines a novel

conserved epitope (Figure 4C) encompassing i) the β3 strand at the N-terminus of GP1, and ii) β19/β20 strands forming the stem of the IFL on GP2. The most critical residues within the CA45 epitope, R64, Y517, and G546, line up in a cluster along the IFL, between the KZ52 binding site and the fusion peptide (the IFL tip) (Figure 4D). The ability to simultaneously bind both GP1 and GP2 is shared between CA45 and base binders. Interestingly, another IFL mAb, FVM02, that interact with residues within the fusion peptide but no GP1 contact has no neutralizing activity (Keck et al., 2015). These data suggest that clamping GP1 and GP2 at the bottom of the trimer may be critical for effective neutralization of ebolaviruses.

In the crystal structure of EBOV GP (5JQ3) (Zhao et al., 2016), a cluster of residues, D192-F193-F194, within the cathepsin cleavage loop hovers over the CA45 epitope. We found that alanine substitution of these residues enhances GP binding to CA45, suggesting that these residues may restrict access to the CA45 epitope in the GP trimer. Interestingly, this region is not traceable in the GP_{CL} structure suggesting that it is either highly disordered or is removed by thermolysin (Bornholdt, 2016), possibly explaining the dramatically increased binding affinity of GP_{CL} for both mature and germline CA45. Mutagenesis of these residues and cleavage by cathepsin may have similar effects on exposure of the CA45 epitope. The ability of this so called "DFF lid" to block access to both the viral GP inhibitor toremifene (Zhao et al., 2016) and CA45 binding sites further suggests that this epitope is a major site of vulnerability and that CA45 and toremifene may be acting by a shared, yet to be defined, mechanism of action. Beside the DFF lid, alanine substitution of the key sites for N40 glycosylation, (N40A and T42A) (Lee et al., 2008), also increased CA45 binding. Collectively, these data strongly suggest that modifying the exposure of such epitopes may help expand the breadth of ebolavirus vaccines.

While CA45 binds close to the base epitope and, like base-binders, contacts both GP2 and GP1, the mechanistic differences between these two classes of antibodies are striking. CA45 appears to function at two levels; partially inhibiting the GP cleavage, an early critical step

in filovirus entry, and blocking the virus entry post-cleavage while KZ52 is completely inactive towards the pre-cleaved EBOV. These observations, along with our live cell imaging data suggest a two-punch mechanism of action by CA45 on early and late stages of the entry process. However, the details of this mechanism remain to be further investigated.

CA45 displayed remarkable efficacy against EBOV infection in mice, with significant protection at a single dose as low as 10 μg/mouse administered at the peak of viremia. Furthermore, in a highly stringent guinea pig model, where animals receive a single dose of up to 5 mg mAb at 3 dpi, CA45 alone provided 50% protection with much lower average weight loss compared to controls. We previously reported on another ebolavirus bNAb, FVM04, that neutralizes EBOV, SUDV, and to a lesser extent BDBV, by binding to the RBS (Howell et al., 2016). Given the distinct mechanisms of action of CA45 and FVM04 at distinct stages of the entry process, we hypothesized that a cocktail of the two mAbs would be more effective. Consistent with this hypothesis, combining FVM04 and CA45 fully protected guinea pigs against EBOV infection with no weight loss or other signs of disease. In an $IFNAR^{-/-}$ mouse model, both CA45 and FVM04 provided strong and nearly complete protection against wild type (non-adapted) SUDV. While mice treated with individual mAbs showed considerable weight loss, animals receiving the CA45/FVM04 cocktail showed consistent weight gain and no apparent signs of disease. In guinea pigs, CA45 alone was fully protective against GPA-SUDV, similar to the protection afforded by FVM04 (Howell et al., 2016). A lethal ferret model was recently developed for filoviruses that recapitulates key hallmarks of the human disease, including hematological, blood chemistry, and coagulation abnormalities as well as petechial rash at the time of death (Kozak et al., 2016). We show that two doses of the CA45/FVM04 cocktail were fully protective in BDBV infected ferrets, evident by the lack of mortality and absence of all clinical and laboratory symptoms of the disease except for a transient low viremia in two of the

animals. This is the first report of a post-exposure antibody therapeutic that is fully protective against all three highly pathogenic ebolaviruses.

During infection, ebolaviruses produce large amounts of nonstructural soluble GP (sGP), the product of the unedited GP gene that lacks MLD and GP2 (de La Vega et al., 2015). sGP is considered a decoy antigen that absorbs antibodies targeted to the apex of the GP trimer. It has been shown, in a naturally infected person, that the majority of the GP-specific B cells produce sGP-binding antibodies (Bornholdt et al., 2016). While a direct role for sGP in pathogenesis has been postulated, there is limited evidence to-date supporting this hypothesis (de La Vega et al., 2015). On the other hand, currently all antibody cocktails that significantly protected against EBOV in NHPs include an sGP binding antibody (Corti et al., 2016; Pettitt et al., 2013; Qiu et al., 2016; Qiu et al., 2012; Qiu et al., 2014). Thus, it remains enigmatic whether sGP binding is a positive or negative attribute of an immunotherapeutic cocktails targeting ebolaviruses. Our findings suggest that the addition of an sGP-cross reactive, RBS-binding mAb such as FVM04 significantly improves the protective efficacy against EBOV. It is possible that a fraction of FVM04 is absorbed by sGP and only the excess FVM04 that is not bound by sGP is responsible for improved efficacy. Alternatively, FVM04 may neutralize a yet to be defined function of sGP that could play a role in ebolavirus pathogenicity. An sGP-binding therapeutic mAb may also relieve the emerging apex binding antibodies produced by the host, which could help control the infection.

In summary, we here report a novel and broadly conserved ebolavirus neutralizing epitope exploited by bNAb CA45, which overlaps with the ebolavirus internal fusion loop. We further demonstrate that an antibody cocktail targeting this epitope together with the receptor binding site can provide broad protection against all three ebolaviruses that have epidemic potential and high mortality in humans. Furthermore, we show that modifications of the GP immunogen to enhance accessibility of antigenic surfaces in the base region of GP can

substantially enhance the reactivity to the bNAb CA45 and its inferred germline precursors, an important finding that can inform better design of broadly protective filovirus vaccines.

EXPERIMENTAL PROCEDURES

Animal samples

The sera and peripheral blood mononuclear cells (PBMC) described in this study were collected from a cynomolgus macaque (macaque 20667), who received three immunizations (on days 0, 28, and 56) with a mixture of filovirus GPΔmuc. The time point of the PBMCs used for the subsequent single B cell sorting was day 84, 28 days post the 3rd immunization. Detailed information on these has been previously reported (Keck et al., 2015).

Isolation of mAbs by single cell sorting

Pan-ebola GP-specific memory B-cell sorting and Ig encoding gene PCR amplification was performed following a previously described macaque single memory B cell sorting and cloning method with modifications (Sundling et al., 2012; Wang et al., 2016b). Briefly, PBMC were incubated with a cocktail of antibodies to CD3 (APC-Cy7; SP34-2, BD Pharmingen), CD8 (Pacific blue; RPA-T8, BD Pharmingen), CD14 (BV605; M5E2, BD Horizon), CD20 (PE-Alexa Fluor 700; 2H7, VRC), CD27 (PE-Cy7; M-T271, BD Pharmingen), IgG (FITC; G18-145, BD Pharmingen), and IgM (PE-Cy5; G20-12, BD Pharmingen), and Aqua blue (Invitrogen) to exclude dead cells. EBOV GPΔmuc with His-tag and SUDV GPΔmuc with HA-tag, produced in insect cell and mammalian 293F cells, respectively, were also used to identify antigen-specific memory B cells at 4 µg/mL in the cocktail. After 1 hour of staining at 4^{o}C, the cells were washed with cold PBS and 10 µL of each of anti-His-PE and anti-HA-APC (Miltenyi) were added in total volume of 100 µL for 1 hour at 4^{o}C. Cross-reactive GP-specific memory B cells were sorted on a FACS Aria III cell sorter (BD Biosciences) to obtain single cells with the phenotype of CD20^{+}IgG^{+}CD14^{-} Aqua Blue^{-}CD3^{-}CD8^{-}CD27^{+}IgM^{-}EBOV_GPΔmuc-PE^{hi}SUDV_GPΔmuc-APC^{hi}. Single cells were sorted into 96-well PCR plates containing lysis buffer followed by single B-cell

RT-PCR. We performed cloning and expression of IgGs using the previously described method (Tiller et al., 2008).

Expression and purification of antibody, Fab fragment, and GP proteins

The genes of CA45 heavy chain, light chain, were cloned into IgG1 expression vectors, produced in FreeStyle™ 293F cells, and purified by protein A column (GE Healthcare Life Sciences) following the manufacturer's protocol as described previously (Wang et al., 2016b). CA45 Fab was prepared by subcloning the heavy-chain gene into a Fab expression vector with an additional 6xHis-tag to the C-terminus (Tran et al., 2014). All proteins were further purified by size exclusion chromatography (SEC). GP protein expression was performed as previously described (Howell et al., 2016). Cleaved GP was produced by thermolysin cleavage of EBOV GPΔTM as previously described (Hashiguchi et al., 2015).

ELISA binding assays: Filovirus glycoproteins lacking the transmembrane domain (GPΔTM), were coated onto 96-well Maxisorb ELISA plates overnight at 4 °C. On the following day, the plates were washed and blocked with StartingBlock Buffer (Thermo Scientific) to each well for 1 hour at room temperature. After blocking, plates were washed again before adding CA45 diluted into 1X DPBS + 0.05% Tween-20 at pH 7.5, 5.5 or 4.5 for 1 hour at room temperature. After incubation, a 1:3000 dilution of Goat Anti-human-HRP (KPL) diluted in blocking buffer was added for 1 hour at room temperature before a final wash and the addition of TMB substrate (Life Technologies). Plates were read for O.D. at 650 nm on a VersaMax plate reader. Softmax was used to fit the data to a 4PL curve.

BioLayer Interferometry (BLI)

Kinetics experiments were performed using the ForteBio Octet Red96 platform. Data were collected at 25°C with orbital shaking at 1,000 rpm in 200 µL volume. Protein G sensors (ForteBio) were equilibrated in 1X kinetics buffer (1X PBS, 0.1% BSA and 0.02% Tween-20) for

10 min prior to loading with 5 µg/mL of CA45 for 2 min. After the loading step, a 30 sec baseline was established before association with a range of concentrations of GPΔTM for EBOV, SUDV, BDBV, or RESTV or EBOV GP_{CL} for 5 min. Following the CA45 association with GP, there was a 10 min of dissociation step in kinetics buffer. A reference sensor without glycoprotein was used to account for nonspecific binding of CA45 to the sensor. The data was fit globally to a 1:1 Langmuir binding model using data analysis software 9.0 (ForteBio).

rVSV GP-GFP Neutralization Assay

Recombinant Indiana VSV (rVSV) expressing eGFP filovirus GP were generated as previously described (Howell et al., 2016; Miller et al., 2012; Ng et al., 2014; Wong et al., 2010). VSV pseudotypes with cleaved GP (GP_{CL}) were generated by incubating pseuodtype bearing full-length GP and incubating for 1 hour with thermolysin at 37°C for 1 hour followed by quenching with phosphoramidon. For neutralization, rVSV-GP was incubated with mAbs in serial dilutions for 1 hour at room temperature before infecting a monolayer of vero cells in 96-well plates. Infectivity of rVSVs were measured by counting eGFP-positive cells 12-14 hours post infection and normalized to control wells without antibody.

rVSV-GP Luciferase Neutralization Assay

Neutralization assays were performed as previously described (Howell et al., 2016). Briefly, vero cells were seeded at 60,000 cells/well overnight. The next day, a serial dilution of CA45 was incubated with pseudotyped virus in serum free media for 1 hour at room temperature before infecting vero cells at an MOI of 0.04 at 37°C for 1 hour. After infection, EMEM medium supplemented with 2% heat inactivated FBS was added to cells. The next day, cells were lysed with passive lysis buffer (Promega) for 30 min at room temperature before the addition of the luciferase activating agent (Promega). The luminesce was read immediately on a Biotek Plate

reader. Percent neutralization was based on well containing virus only. Data was fit to a 4PL curve in GraphPad Prism 6.

Gene family usage of IgG gene

The gene family usage of the variable region of the IgG heavy- and light- chains was analyzed using IgBlast (http://www.ncbi.nlm.nih.gov/igblast/) with KABAT as the V domain delineation system and a customized cynomolgus macaques Ig heavy- and light- chain germline database annotated based on the published cynomolgus macaques genomic data set (Ebeling et al., 2011; Yan et al., 2011; Yu et al., 2016).

CA45 heavy- and light-chains Ala scanning:

A panel of 63 alanine (Ala) mutants of CA45 was generated, with each amino acid residue in the heavy chain and light chain complementarity-determining regions (CDRs; subdomain delineated by Kabat system through IgBlast as described above) substituted by Ala, with the exception of Ala residues already present in the WT sequence. Each mutant HC or LC was paired with their corresponding WT HC or LC and co-transfected into FreeStyle™ 293F cells, with the culture supernatants collected four days later for binding analysis.

The dilution factor of the Ala mutant supernatants has been optimized by pilot ELISA to reach OD450 value from 0.6-1.5. Maxisorp ELISA plates (Nunc) were coated with 2 µg/mL of GP proteins (EBOV, SUDV or BDBV) for detecting GP binding or AffiniPure Donkey anti-Human IgG, Fcγ fragment (Jackson ImmunoResearch Labs) for normalizing IgG expression, respectively in PBS (pH 7.4) at 4°C overnight. After incubation with blocking buffer (BB, 2% non-fat milk, 5% FBS in PBS), the WT or mutant supernatant in five-fold serial dilution in BB was added and incubated for 1 hour at 37°C. The secondary Ab, HRP-conjugated goat anti-human Fab (Jackson ImmunoResearch Labs), and TMB solution (Life Technologies) were used to develop signal. OD450 value for GP-bindings were normalized with corresponding IgG

expression OD450 value, and relative GP binding affinity were calculated for each Ala mutant compared with the WT supernatant value.

Epitope mapping of GP using alanine scanning mutagenesis

A shotgun mutagenesis library of EBOV GP expressed in HEK-293 cells was used to determine the critical GP residues for rCA45 binding. Details of the method were previously described (Howell et al., 2016).

Electron Microscopy (EM), Image processing and 3D reconstruction

EBOV GPΔTM was incubated with 6 molar excess of CA45 Fab overnight at 4°C. The complex was purified through an S200i SEC column (GE Healthcare). The sample was added to 400 square copper mesh grids coated with carbon and stained with 2% uranyl formate. The grids were imaged on a 120keV Tecnai Spirit electron microscope using a TemCam F416 4k x 4k CCD. Particles were selected from raw micrographs using DoGPicker (Voss et al., 2009) through the Appion interface (Lander et al., 2009). Particles were then organized into stacks and aligned using iterative MRA/MSA (Ogura et al., 2003). After making clean 2D stack of particles, EMAN2 (Tang et al., 2007) was used to refine a final 3D model. Crystal structures were docked into the reconstruction using UCSF Chimera (Pettersen et al., 2004).

Cathepsin cleavage inhibition assay:

The viral envelope of rVSV-EBOV GP virions were labeled with biotin using a function-spacer-lipid construct (FSL-biotin) (Sigma-Aldrich) at neutral pH for 1h at 37°C, as described previously (Ng et al., 2014). The labeled virus stock was then acidified to pH ~5.5 by addition of 10X MES buffer. Virions were diluted and aliquoted into a PCR plate. Biotin-labeled virions were pre-incubated with 1000 nM of test antibody for one hour at 37°C at pH 5.5. Virion-antibody complexes were then subjected to proteolysis by recombinant human Cathepsin L (R&D

Systems) at 4 ng/µL for 30 mins at 37°C. The reaction was stopped by addition of E64 inhibitor (Peptides International) followed by dilution into 1XPBS buffer, pH 7.4. Samples were analyzed by western blotting using h21D10 monoclonal antibody (Holtsberg et al., 2015) directly conjugated to horseradish peroxidase.

Live Cell Imaging

Live imaging was performed as previously described on a Zeiss AxioObserver.Z1 widefield epifluorescence microscope equipped with a heated environmental chamber, 40x/1.3NA objective, and DAPI/FITC/Texas Red/Cy5 filters (Spence et al., 2016). Briefly, purified DiD-labeled VSV expressing full-length EBOV GP was incubated with 100 µg/mL CA45 in imaging buffer for 1 h at 37^{o}C. Virus was spinoculated at 4^{o}C and 1500 x g for 20 min onto pre-chilled U2OS cell monolayers seeded on glass coverslip dishes (MatTek). Following the removal of unbound virus, dishes were immediately mounted in the microscope, and warm imaging buffer was added to mark the start of experiments. Images were taken every 6 seconds over a 2 h period. To examine viral trafficking, antibody-treated DiD-labeled virus was spinoculated onto U2OS cells stably expressing monomeric NeonGreen-tagged NPC1. Cells were imaged live at 45 min after warming to 37^{o}C. Data were compiled from three independent experiments, and co-localization analysis was performed using Volocity (Perkin Elmer) software as described previously (Spence et al., 2016).

Animal studies

Mouse challenge studies with EBOV: 6-8 week old, female BALB/c mice were given 100 PFU of mouse-adapted EBOV (Mayinga) diluted in PBS, via the IP route. Antibodies were administered IP at indicated time points and dosage. Control mice were given PBS. Mice were observed through day 21 for clinical signs of disease such as hypoactivity, reduced grooming, and weight loss. When signs of disease were noted, observations were increased to two times a day.

Moribund and surviving mice were humanely euthanized accordingly to IACUC-approved criteria.

Mouse challenge study with SUDV: male and female IFNAR$^{-/-}$ mice (4-5 weeks old) were exposed by IP infection to 1,000 PFUs of SUDV (Boniface) and treated with antibodies at indicated time points and doses. Control mice were given PBS. Mice were observed for clinical signs of disease daily and moribund and surviving mice were humanely euthanized according to IACUC-approved criteria.

Guinea pig challenge studies with EBOV and SUDV: 4-6 week old female Hartley guinea pigs (250-300 g) were challenged via IP with a 1000 x LD_{50} of guinea pig adapted EBOV or 1000 x LD_{50} guinea pig adapted SUDV in 1 mL of DMEM. CA45 and/or FVM04 were given at indicated time points and doses, with 6 guinea pigs/group (n=6). Control guinea pigs with 4 animals/group (n=4), were given PBS treatment. Animal were observed for clinical signs of disease, survival and weight change for 15-16 days, while survival was monitored for an additional 12 days.

Ferrets challenge studies with BDBV:

Ferret challenge studies were performed as previously described (Kozak et al., 2016). Briefly, 6-month old male and female ferrets (Mustela putorius furo) (620-960 g) were infected by intramuscular route with 253 $TCID_{50}$ of Bundibugyo virus/H.sapiens-wt/UGA/2007 (BDBV, Genbank accession number KR063673.1). Animals were monitored daily and clinical scoring was recorded. Blood, oral, and rectal swabs, and nasal wash samples were collected at -1, 3, 6, 10, 14, 21, and 27 dpi. Blood cell counts and serum chemistry assays were performed following the manufacturer's instructions using a VetScan HM5 hematology machine (Abaxis, USA) and VetScan VS2 analyzer (Abaxis, USA), respectively. Viral RNA was extracted using the QIAamp viral RNA mini kit (Qiagen) following the manufacturer's instructions. Samples viral loads were determined using reverse transcription quantitative PCR (RT-qPCR) with an ABI StepOnePlus instrument as described previously (Kozak et al., 2016).

Ethics statement. Animal research using mice was conducted under a protocol approved by the US Army Medical Research Institute of Infectious Diseases (USAMRIID) Institutional Animal Care and Use Committee (IACUC) in compliance with the Animal Welfare Act and other federal statutes and regulations relating to animals and experiments involving animals. The USAMRIID facility is fully accredited by the Association for the Assessment and Accreditation of Laboratory Animal Care International and adheres to the principles stated in the Guide for the Care and Use of Laboratory Animals (National Research Council. Guide for the care and use of laboratory animals. 8th ed. Washington, DC: National Academies Press, 2011). Challenge studies were conducted under maximum containment in an animal biosafety level 4 facility. The guinea pig and ferret experiments were performed at the National Microbiology Laboratory in Winnipeg, Manitoba, Canada. All animal experiments have been approved by the Animal Care Committee at the Canadian Science Center for Human and Animal Health in accordance with the guidelines outlined by the Canadian Council on Animal Care.

Statistical analysis: For animal studies, Kaplan Meier survival curves were analyzed with the log-rank (Mantel-Cox) test using GraphPad Prism software. Individual animal experiments were performed with 10 mice per group (n=10). In some instances, data from multiple experiments with identical conditions are combined in one Kaplan Meier curve and analyzed statistically (where indicated in figure legends with n>10). For alanine scanning mutagenesis of GP the error bars represent the mean and range of at least two replicate data points. For ELISA and neutralization data each data point is represented as average of triplicates ±SD.

Acknowledgements

This work was supported by a contract (HDTRA1-13-C-0015) from US Defense Threat Reduction Agency (DTRA) and a grant (R43AI124765) from National Institute of Allergy and Infectious Diseases to MJA, Intramural Research Award from the Institute for Bioscience and Biotechnology Research, University of Maryland to YL, and NIH contract HHSN272201400058C

to BJD. This work was also partially supported by Public Health Agency of Canada (PHAC). Opinions, interpretations, conclusions, and recommendations are those of the authors and are not necessarily endorsed by the U.S. Army. The mention of trade names or commercial products does not constitute endorsement or recommendation for use by the Department of the Army or the Department of Defense.

Figure Legends:

Figure 1: Isolation of broadly neutralizing mAb CA45 from GP-immunized cynomolgus macaque.

(A) The neutralizing capacity of the serum of GP-immunized cynomolgus macaque, 20667, at week 12 (28 days post the 3rd immunization) was assessed against pseudotyped VSV-GP-Luc for EBOV, SUDV and BDBV. (B) Single B cell sorting of cross-reactive GP-specific mAbs by flow cytometry. PBMCs from week 12 time point were incubated with cell markers and sorting probes consisting of EBOV and SUDV GPΔmuc. Cross-reactive memory B cells with the phenotype of CD20^{+}IgG^{+}Aqua blue^{-}CD14^{-}CD3^{-}CD8^{-}CD27^{+}IgM$^{-)}$ as well as dual reactivity with GPs (EBOV GPΔmuc^{hi} SUDV GPΔmuc^{hi}) were sorted into 96-well microtiter plates for Ig heavy- and light-chain gene amplification. (C) Initial validation of GP cross-reactive mAb FACS sorting and cloning precision by ELISA binding assay. IgG1 molecules from 12 selected sorted cells were expressed with paired heavy- and light-chain genes and tested for binding specificity for EBOV and SUDV GPΔmuc. >90% cloned mAb IgGs were positive for both GP ligands. Also see Tables S1 and S2.

Figure 2: Binding characteristics and neutralizing activity of CA45.

(A) Reactivity of CA45 to glycoprotein ectodomains (GPΔTM) of EBOV, SUDV, BDBV, and RESTV, as well as EBOV GP_{CL} and sGP determined by ELISA at neutral and acidic pH. EC_{50} values (nM) for each antigen and pH condition are shown**.** (B) Kinetics of CA45 binding analyzed by BLI. The sensograms show the association and dissociation curves for binding of GPΔTM of EBOV, SUDV, or BDBV as well as EBOV GP_{CL} to CA45 immobilized on protein G sensors. Analyzed concentration ranges are indicated (colored) and the fits are shown as dashed lines. On-rate (k_{on}), off-rate (k_{off}), and K_D values for each GP ligand are shown below the sensograms. (C) CA45 neutralization capacity against ebolaviruses: *far left)* pseudotyped

replication competent rVSV-GFP-TAFV, -LLOV, -RESTV, -EBOV, -SUDV, and –BDBV produced in Vero cells; *left*) pseudotyped replication incompetent rVSV-Luc-EBOV, -SUDV, and –BDBV produced in Vero cells; *middle)* CA45 mediated neutralization of thermolysin cleaved rVSV-GFP-GP (subscript CL) in comparison to non-cleaved rVSV-GFP-GP; *right*) replication competent ebolaviruses. Also see Figure S1**.**

Figure 3: CA45 heavy- and light-chain gene sequence, critical residues for GP recognition and clonal affinity maturation.

(A) Sequence analysis of CA45 heavy and light chains with alignment to respective cynomolgus macaque Ig germline gene (V-(D)-J) segments as well as the N region that serves as the junction between VH-DH and DH-JH segments. (B) Alanine scanning mutants of CA45 heavy (HC, left) and light chain (LC, right) CDR loops were assessed for binding affinity for EBOV GPΔmuc relative to the wildtype (WT) IgG molecule. Mutated residues with relative binding signal < 0.33 (with relative affinity decreases more than 3-folds) were considered to be critical for EBOV GP binding. (C) Summary of CA45 heavy- (left) and light-chain (right) CDR loop critical residues for EBOV, SUDV and BDBV binding. Critical residues for GP binding (with the same criterion as in (B) are highlighted in blue. (D) Summary of binding kinetics of CA45 and its germline precursors to various GP ligands. CA45-$H_{GL}L_{GL}$ consists of CA45 germline reverted heavy- and light-chain; CA45-H_mL_{GL} consists of CA45 matured heavy chain and germline reverted light chain; GP_{CL}, GPΔTM molecule with glycan cap removed by cysteine cathepsins. NB, no binding. Also see Figure S3 and Table S3.

Figure 4: CA45 Epitope mapping.

(A) The EBOV GP shotgun mutagenesis alanine substitution library was tested for reactivity with CA45. Clones with <25% binding relative to that of wild-type (WT) EBOV GP yet >65% reactivity for a control mAb were initially identified to be critical for CA45 binding are highlighted in red. (B) Mutations of four individual residues reduced CA45 binding (red bars) but retained FVM04 and

FVM09 binding (gray bars). Bars represent the mean and range of at least two replicates. (C) Homology between filovirus GP sequences within the regions encompassing the CA45 epitope. Conserved residues are shown in blue and CA45 critical residues in red. Arrows show the corresponding beta strands in EBOV GP structure. (D) Position of GP residues critical for CA45 in the structure of trimeric EBOV GP, highlighted in a circle with a dashed line. Also see Table S4, and Figures S4 and S5.

Figure 5. Single-particle electron microscopy (EM) analysis of CA45 Fab bound to EBOV GPΔMuc

(A) 3D EM reconstruction of CA45 Fab bound to EBOV GPΔMuc (gray) with crystal structure of EBOV GPΔMuc (light blue, PDB 5JQ3) docked in. (B) The same EM map with a single EBOV GP protomer docked in with the internal fusion loop (IFL) highlighted in dark blue. (C) Light (orange) and heavy chain (purple) of CA45 Fab homology model docked into EM map. The CDRH1 and CDRH3 of CA45 were docked in close proximity to GP, based on the CA45 CDR ala scanning data in Figure 3C. GP residues, R64, Y517, G546, and N550 that are important in CA45 binding are highlighted in dark blue spheres, K190 in light blue spheres. (D) Comparison of CA45 and KZ52 epitopes. *Upper*, bottom view of the EM map with crystal structure of KZ52 Fab bound to EBOV GP protomer (PMD 5HJ3) with the epitope highlighted in red. *Middle***,** the CA45 Fab epitope (purple) includes overlapping residues (yellow) with the epitope of KZ52. *Lower*, The GP residues contacted by KZ52 are less conserved between various Filoviridae compared to CA45. (E) Comparison of Ebola GP interactions with cross-protective mAb CA45 and other Ebola strain-specific neutralizing antibodies (KZ52, c2G4, and c4G7) at the GP1-GP2 interface. *Left*, top view. *Right*, side view. c2G4 Fab in yellow (EMD-6151), c4G7 Fab in purple (EMD-6152) are part of ZMapp^{TM}. KZ52 crystal structure (PDB 5HJ3) in blue also contacts similar residues as c2G4. CA45 Fab (gray) has significant overlap with these three EBOV

antibodies, but with its shifted angle of approach, may confer breadth of neutralization. Also see Figure S6.

Figure 6: Efficacy in mouse and guinea pig models

(A) Groups of 10 or 20 BALB/c mice were infected with 100 pfu of MA-EBOV and treated with a single IP injection of CA45 at indicated doses or PBS as control at 2 dpi and monitored for 21 days. *p* values for each treatment group compared to the PBS group was determined by Log-rank (Mantel-Cox) test. (B) $IFNAR^{-/-}$ mice were infected with 1000 pfu of wild type SUDV and treated at 1 dpi with a single IP injection of either PBS as control, FVM04, CA45, or combination of the two mAbs at indicated doses. Animals were monitored for 21 days. Data in the upper panel are combined from two experiments (C) Hartley guinea pigs were infected with 1000 LD_{50} of GPA-EBOV and treated at 3 dpi by IP injection of FVM04, CA45, or the cocktail (n=6 each) or PBS (n=4). Animals were monitored for 28 days. *p* values: CA45 vs. PBS, p =0.0018; FVM04 vs. PBS, p=0.0018; cocktails vs. PBS p<0.0001; CA45 vs. cocktails, p=0.0079; FVM04 vs. cocktails, p<0.0001. (D) Guinea pigs were challenged with GPA-SUDV and treated with 5 mg of CA45 (n=6) or PBS (n=4) at 3 dpi and monitored for 28 days, p<0.0001.

Figure 7: Efficacy in ferret model of BDBV infection

Groups of two male and two female ferrets (denoted with M or F suffix to animal number) were infected with 253 $TCID_{50}$ of BDBV followed by IP treatment at 3 and 6 dpi with 20 mg of CA45 and FVM04. Two control animals (780M and 727F) received PBS only. Protection data are shown as percent survival (A), clinical score (B), weight change (C), viral burden in blood (D), and tissue swabs (E-G), as well as blood chemistry markers (H-L). Also see Figure S7.

References

Bornholdt, Z.A., Ndungo, E., Fusco, M.L., Flyak, A.I., Crowe, J.E., Chandran, K., and Saphire, E.O. (2016). Host-primed Ebola virus GP exposes a hydrophobic NPC1 receptor-binding pocket, revealing a target for broadly neutralizing antibodies. MBio *In Press*.

Bornholdt, Z.A., Turner, H.L., Murin, C.D., Li, W., Sok, D., Souders, C.A., Piper, A.E., Goff, A., Shamblin, J.D., Wollen, S.E*., et al.* (2016). Isolation of potent neutralizing antibodies from a survivor of the 2014 Ebola virus outbreak. Science *351*, 1078-1083.

Brannan, J.M., Froude, J.W., Prugar, L.I., Bakken, R.R., Zak, S.E., Daye, S.P., Wilhelmsen, C.E., and Dye, J.M. (2015). Interferon alpha/beta Receptor-Deficient Mice as a Model for Ebola Virus Disease. J Infect Dis.

Bray, M., Davis, K., Geisbert, T., Schmaljohn, C., and Huggins, J. (1999). A mouse model for evaluation of prophylaxis and therapy of Ebola hemorrhagic fever. J Infect Dis *179 Suppl 1*, S248-258.

Carette, J.E., Raaben, M., Wong, A.C., Herbert, A.S., Obernosterer, G., Mulherkar, N., Kuehne, A.I., Kranzusch, P.J., Griffin, A.M., Ruthel, G*., et al.* (2011). Ebola virus entry requires the cholesterol transporter Niemann-Pick C1. Nature *477*, 340-343.

Chandran, K., Sullivan, N.J., Felbor, U., Whelan, S.P., and Cunningham, J.M. (2005). Endosomal proteolysis of the Ebola virus glycoprotein is necessary for infection. Science *308*, 1643-1645.

Chen, G., Koellhoffer, J.F., Zak, S.E., Frei, J.C., Liu, N., Long, H., Ye, W., Nagar, K., Pan, G., Chandran, K*., et al.* (2014). Synthetic antibodies with a human framework that protect mice from lethal Sudan ebolavirus challenge. ACS Chem Biol *9*, 2263-2273.

Corti, D., Misasi, J., Mulangu, S., Stanley, D.A., Kanekiyo, M., Wollen, S., Ploquin, A., Doria-Rose, N.A., Staupe, R.P., Bailey, M*., et al.* (2016). Protective monotherapy against lethal Ebola virus infection by a potently neutralizing antibody. Science.

Davidson, E., Bryan, C., Fong, R.H., Barnes, T., Pfaff, J.M., Mabila, M., Rucker, J.B., and Doranz, B.J. (2015). Mechanism of Binding to Ebola Virus Glycoprotein by the ZMapp, ZMAb, and MB-003 Cocktail Antibodies. J Virol *89*, 10982-10992.

de La Vega, M.A., Wong, G., Kobinger, G.P., and Qiu, X. (2015). The multiple roles of sGP in Ebola pathogenesis. Viral Immunol *28*, 3-9.

Dias, J.M., Kuehne, A.I., Abelson, D.M., Bale, S., Wong, A.C., Halfmann, P., Muhammad, M.A., Fusco, M.L., Zak, S.E., Kang, E*., et al.* (2011). A shared structural solution for neutralizing ebolaviruses. Nat Struct Mol Biol *18*, 1424-1427.

Diehl, W.E., Lin, A.E., Grubaugh, N.D., Carvalho, L.M., Kim, K., Kyawe, P.P., McCauley, S.M., Donnard, E., Kucukural, A., McDonel, P*., et al.* (2016). Ebola Virus Glycoprotein with Increased Infectivity Dominated the 2013-2016 Epidemic. Cell *167*, 1088-1098 e1086.

Ebeling, M., Kung, E., See, A., Broger, C., Steiner, G., Berrera, M., Heckel, T., Iniguez, L., Albert, T., Schmucki, R*., et al.* (2011). Genome-based analysis of the nonhuman primate Macaca fascicularis as a model for drug safety assessment. Genome Res *21*, 1746-1756.

Feldmann, H., and Geisbert, T.W. (2011). Ebola haemorrhagic fever. Lancet *377*, 849-862.

Flyak, A.I., Shen, X., Murin, C.D., Turner, H.L., David, J.A., Fusco, M.L., Lampley, R., Kose, N., Ilinykh, P.A., Kuzmina, N*., et al.* (2016). Cross-Reactive and Potent Neutralizing Antibody Responses in Human Survivors of Natural Ebolavirus Infection. Cell *164*, 392-405.

Hashiguchi, T., Fusco, M.L., Bornholdt, Z.A., Lee, J.E., Flyak, A.I., Matsuoka, R., Kohda, D., Yanagi, Y., Hammel, M., Crowe, J.E., Jr*., et al.* (2015). Structural basis for marburg virus neutralization by a cross-reactive human antibody. Cell *160*, 904-912.

Holtsberg, F.W., Shulenin, S., Vu, H., Howell, K.A., Patel, S.J., Gunn, B., Karim, M., Lai, J.R., Frei, J.C., Nyakatura, E.K*., et al.* (2015). Pan-ebolavirus and Pan-filovirus Mouse Monoclonal Antibodies: Protection against Ebola and Sudan Viruses. J Virol *90*, 266-278.

Howell, K.A., Qiu, X., Brannan, J.M., Bryan, C., Davidson, E., Holtsberg, F.W., Wec, A.Z., Shulenin, S., Biggins, J.E., Douglas, R*., et al.* (2016). Antibody Treatment of Ebola and Sudan Virus Infection via a Uniquely Exposed Epitope within the Glycoprotein Receptor-Binding Site. Cell Rep *15*, 1514-1526.

Jardine, J., Julien, J.P., Menis, S., Ota, T., Kalyuzhniy, O., McGuire, A., Sok, D., Huang, P.S., MacPherson, S., Jones, M*., et al.* (2013). Rational HIV immunogen design to target specific germline B cell receptors. Science *340*, 711-716.

Keck, Z.Y., Enterlein, S.G., Howell, K.A., Vu, H., Shulenin, S., Warfield, K.L., Froude, J.W., Araghi, N., Douglas, R., Biggins, J*., et al.* (2015). Macaque Monoclonal Antibodies Targeting Novel Conserved Epitopes within Filovirus Glycoprotein. J Virol *90*, 279-291.

Kozak, R., He, S., Kroeker, A., de La Vega, M.A., Audet, J., Wong, G., Urfano, C., Antonation, K., Embury-Hyatt, C., Kobinger, G.P*., et al.* (2016). Ferrets infected with Bundibugyo virus or Ebola virus recapitulate important aspects of human filoviral disease. J Virol.

Kuhn, J.H., Andersen, K.G., Baize, S., Bao, Y., Bavari, S., Berthet, N., Blinkova, O., Brister, J.R., Clawson, A.N., Fair, J*., et al.* (2014). Nomenclature- and database-compatible names for the two Ebola virus variants that emerged in Guinea and the Democratic Republic of the Congo in 2014. Viruses *6*, 4760-4799.

Lander, G.C., Stagg, S.M., Voss, N.R., Cheng, A., Fellmann, D., Pulokas, J., Yoshioka, C., Irving, C., Mulder, A., Lau, P.W*., et al.* (2009). Appion: an integrated, database-driven pipeline to facilitate EM image processing. J Struct Biol *166*, 95-102.

Lee, J.E., Fusco, M.L., Hessell, A.J., Oswald, W.B., Burton, D.R., and Saphire, E.O. (2008). Structure of the Ebola virus glycoprotein bound to an antibody from a human survivor. Nature *454*, 177-182.

Lee, J.E., and Saphire, E.O. (2009). Neutralizing ebolavirus: structural insights into the envelope glycoprotein and antibodies targeted against it. Curr Opin Struct Biol *19*, 408-417.

McGuire, A.T., Gray, M.D., Dosenovic, P., Gitlin, A.D., Freund, N.T., Petersen, J., Correnti, C., Johnsen, W., Kegel, R., Stuart, A.B*., et al.* (2016). Specifically modified Env immunogens activate B-cell precursors of broadly neutralizing HIV-1 antibodies in transgenic mice. Nat Commun *7*, 10618.

Miller, E.H., Obernosterer, G., Raaben, M., Herbert, A.S., Deffieu, M.S., Krishnan, A., Ndungo, E., Sandesara, R.G., Carette, J.E., Kuehne, A.I*., et al.* (2012). Ebola virus entry requires the host-programmed recognition of an intracellular receptor. EMBO J *31*, 1947-1960.

Mire, C.E., Geisbert, J.B., Marzi, A., Agans, K.N., Feldmann, H., and Geisbert, T.W. (2013). Vesicular stomatitis virus-based vaccines protect nonhuman primates against Bundibugyo ebolavirus. PLoS Negl Trop Dis *7*, e2600.

Misasi, J., Gilman, M.S., Kanekiyo, M., Gui, M., Cagigi, A., Mulangu, S., Corti, D., Ledgerwood, J.E., Lanzavecchia, A., Cunningham, J*., et al.* (2016). Structural and molecular basis for Ebola virus neutralization by protective human antibodies. Science.

Murin, C.D., Fusco, M.L., Bornholdt, Z.A., Qiu, X., Olinger, G.G., Zeitlin, L., Kobinger, G.P., Ward, A.B., and Saphire, E.O. (2014). Structures of protective antibodies reveal sites of vulnerability on Ebola virus. Proc Natl Acad Sci U S A *111*, 17182-17187.

Ng, M., Ndungo, E., Jangra, R.K., Cai, Y., Postnikova, E., Radoshitzky, S.R., Dye, J.M., Ramirez de Arellano, E., Negredo, A., Palacios, G*., et al.* (2014). Cell entry by a novel European filovirus requires host endosomal cysteine proteases and Niemann-Pick C1. Virology *468-470*, 637-646.

Ogura, T., Iwasaki, K., and Sato, C. (2003). Topology representing network enables highly accurate classification of protein images taken by cryo electron-microscope without masking. J Struct Biol *143*, 185-200.

Pettersen, E.F., Goddard, T.D., Huang, C.C., Couch, G.S., Greenblatt, D.M., Meng, E.C., and Ferrin, T.E. (2004). UCSF Chimera--a visualization system for exploratory research and analysis. J Comput Chem *25*, 1605-1612.

Pettitt, J., Zeitlin, L., Kim do, H., Working, C., Johnson, J.C., Bohorov, O., Bratcher, B., Hiatt, E., Hume, S.D., Johnson, A.K.*, et al.* (2013). Therapeutic intervention of Ebola virus infection in rhesus macaques with the MB-003 monoclonal antibody cocktail. Sci Transl Med *5*, 199ra113.

Qiu, X., Audet, J., Lv, M., He, S., Wong, G., Wei, H., Luo, L., Fernando, L., Kroeker, A., Fausther Bovendo, H.*, et al.* (2016). Two-mAb cocktail protects macaques against the Makona variant of Ebola virus. Sci Transl Med *8*, 329ra333.

Qiu, X., Audet, J., Wong, G., Pillet, S., Bello, A., Cabral, T., Strong, J.E., Plummer, F., Corbett, C.R., Alimonti, J.B.*, et al.* (2012). Successful treatment of ebola virus-infected cynomolgus macaques with monoclonal antibodies. Sci Transl Med *4*, 138ra181.

Qiu, X., Wong, G., Audet, J., Bello, A., Fernando, L., Alimonti, J.B., Fausther-Bovendo, H., Wei, H., Aviles, J., Hiatt, E.*, et al.* (2014). Reversion of advanced Ebola virus disease in nonhuman primates with ZMapp. Nature *514*, 47-53.

Saphire, E.O., and Aman, M.J. (2016). Feverish Quest for Ebola Immunotherapy: Straight or Cocktail? Trends Microbiol *24*, 684-686.

Sok, D., Briney, B., Jardine, J.G., Kulp, D.W., Menis, S., Pauthner, M., Wood, A., Lee, E.C., Le, K.M., Jones, M.*, et al.* (2016). Priming HIV-1 broadly neutralizing antibody precursors in human Ig loci transgenic mice. Science *353*, 1557-1560.

Spence, J.S., Krause, T.B., Mittler, E., Jangra, R.K., and Chandran, K. (2016). Direct Visualization of Ebola Virus Fusion Triggering in the Endocytic Pathway. MBio *7*.

Sundling, C., Li, Y., Huynh, N., Poulsen, C., Wilson, R., O'Dell, S., Feng, Y., Mascola, J.R., Wyatt, R.T., and Karlsson Hedestam, G.B. (2012). High-resolution definition of vaccine-elicited B cell responses against the HIV primary receptor binding site. Sci Transl Med *4*, 142ra196.

Tang, G., Peng, L., Baldwin, P.R., Mann, D.S., Jiang, W., Rees, I., and Ludtke, S.J. (2007). EMAN2: an extensible image processing suite for electron microscopy. J Struct Biol *157*, 38-46.

Tiller, T., Meffre, E., Yurasov, S., Tsuiji, M., Nussenzweig, M.C., and Wardemann, H. (2008). Efficient generation of monoclonal antibodies from single human B cells by single cell RT-PCR and expression vector cloning. J Immunol Methods *329*, 112-124.

Tran, E.E., Nelson, E.A., Bonagiri, P., Simmons, J.A., Shoemaker, C.J., Schmaljohn, C.S., Kobinger, G.P., Zeitlin, L., Subramaniam, S., and White, J.M. (2016). Mapping of Ebolavirus Neutralization by Monoclonal Antibodies in the ZMapp Cocktail Using Cryo-Electron Tomography and Studies of Cellular Entry. J Virol.

Tran, K., Poulsen, C., Guenaga, J., de Val, N., Wilson, R., Sundling, C., Li, Y., Stanfield, R.L., Wilson, I.A., Ward, A.B.*, et al.* (2014). Vaccine-elicited primate antibodies use a distinct approach to the HIV-1 primary receptor binding site informing vaccine redesign. Proc Natl Acad Sci U S A *111*, E738-747.

Voss, N.R., Yoshioka, C.K., Radermacher, M., Potter, C.S., and Carragher, B. (2009). DoG Picker and TiltPicker: software tools to facilitate particle selection in single particle electron microscopy. J Struct Biol *166*, 205-213.

Wang, H., Shi, Y., Song, J., Qi, J., Lu, G., Yan, J., and Gao, G.F. (2016a). Ebola Viral Glycoprotein Bound to Its Endosomal Receptor Niemann-Pick C1. Cell *164*, 258-268.

Wang, Y., Sundling, C., Wilson, R., O'Dell, S., Chen, Y., Dai, K., Phad, G.E., Zhu, J., Xiao, Y., Mascola, J.R.*, et al.* (2016b). High-Resolution Longitudinal Study of HIV-1 Env Vaccine-Elicited B Cell Responses to the Virus Primary Receptor Binding Site Reveals Affinity Maturation and Clonal Persistence. J Immunol *196*, 3729-3743.

Yan, G., Zhang, G., Fang, X., Zhang, Y., Li, C., Ling, F., Cooper, D.N., Li, Q., Li, Y., van Gool, A.J., *et al.* (2011). Genome sequencing and comparison of two nonhuman primate animal models, the cynomolgus and Chinese rhesus macaques. Nat Biotechnol *29*, 1019-1023.

Yu, G.Y., Mate, S., Garcia, K., Ward, M.D., Brueggemann, E., Hall, M., Kenny, T., Sanchez-Lockhart, M., Lefranc, M.P., and Palacios, G. (2016). Cynomolgus macaque (Macaca fascicularis) immunoglobulin heavy chain locus description. Immunogenetics *68*, 417-428.

Zhao, Y., Ren, J., Harlos, K., Jones, D.M., Zeltina, A., Bowden, T.A., Padilla-Parra, S., Fry, E.E., and Stuart, D.I. (2016). Toremifene interacts with and destabilizes the Ebola virus glycoprotein. Nature *535*, 169-172.

Figure 1

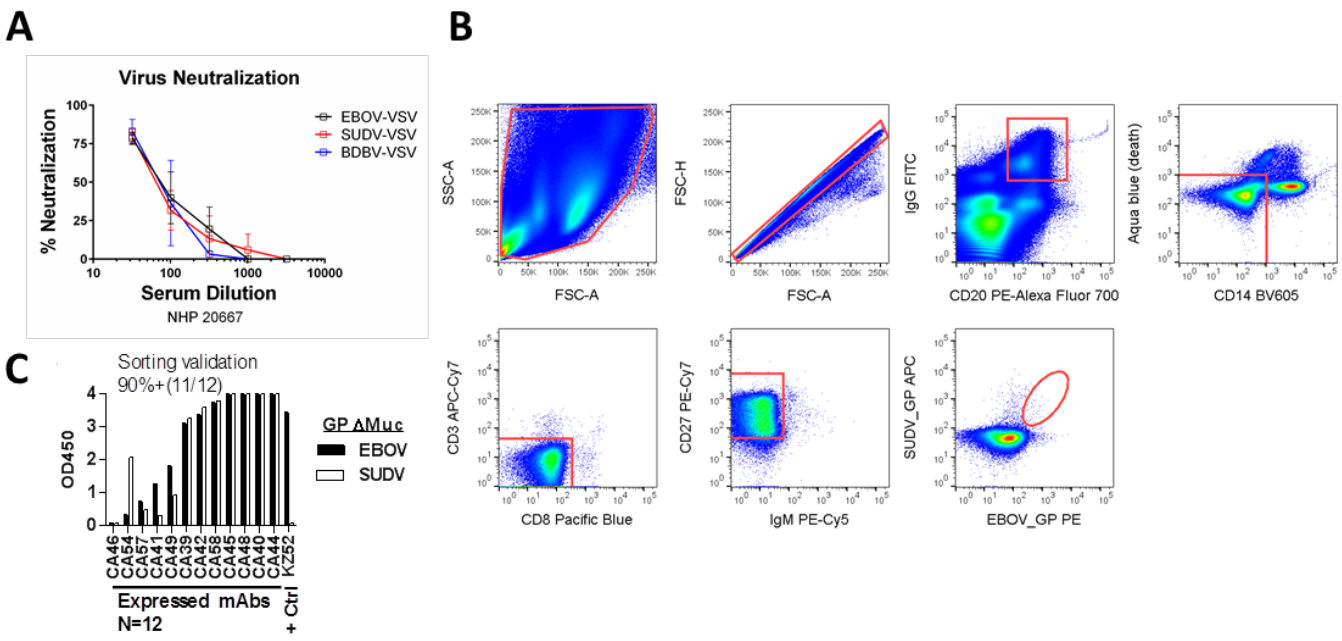
A
Virus Neutralization
% Neutralization
EBOV-VSV
SUDV-VSV
BDBV-VSV
Serum Dilution
NHP 20667
B
SSC-A
FSC-A
FSC-H
FSC-A
IgG FITC
CD20 PE-Alexa Fluor 700
Aqua blue (death)
CD14 BV605
CD3 APC-Cy7
CD8 Pacific Blue
CD27 PE-Cy7
IgM PE-Cy5
SUDV_GP APC
EBOV_GP PE
C
Sorting validation
90%+(11/12)
OD450
GP ΔMuc
EBOV
SUDV
CA46
CA54
CA57
CA41
CA49
CA39
CA42
CA58
CA45
CA48
CA40
CA44
KZ52
Expressed mAbs
N=12
+ Ctrl

Figure 2

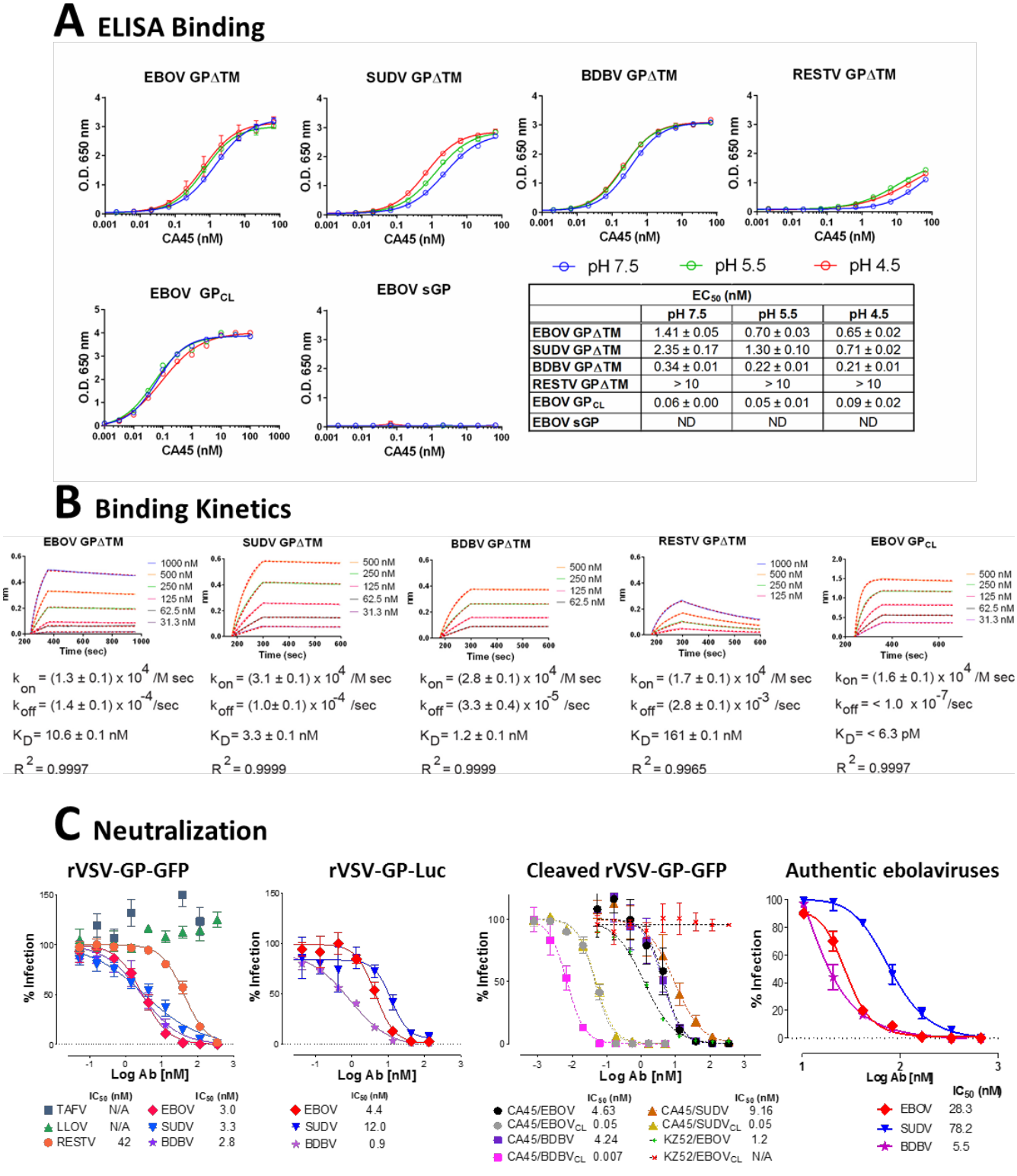

EC50 (nM)	pH 7.5	pH 5.5	pH 4.5
EBOV GPΔTM	1.41 ± 0.05	0.70 ± 0.03	0.65 ± 0.02
SUDV GPΔTM	2.35 ± 0.17	1.30 ± 0.10	0.71 ± 0.02
BDBV GPΔTM	0.34 ± 0.01	0.22 ± 0.01	0.21 ± 0.01
RESTV GPΔTM	> 10	> 10	> 10
EBOV GPCL	0.06 ± 0.00	0.05 ± 0.01	0.09 ± 0.02
EBOV sGP	ND	ND	ND

Figure 3

A

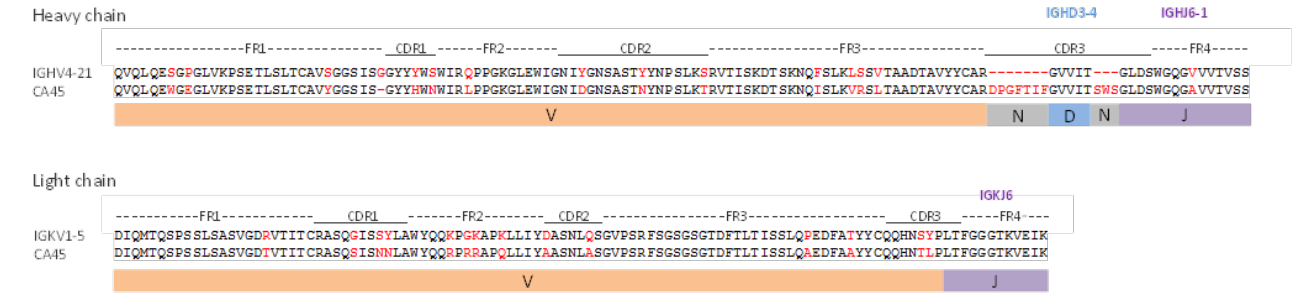

B

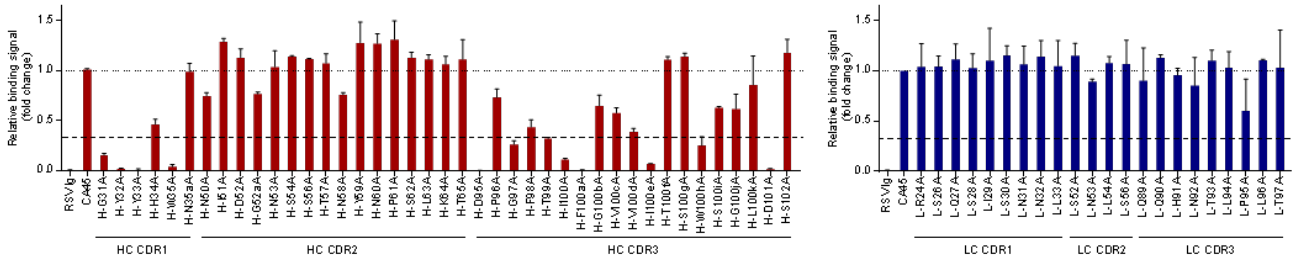

C

Mutations	Binding affinity relative to WT[a] EBOV GPΔMuc	SUDV GPΔMuc	BDBV GPΔTM
CDRH1[b]			
G31A	0.16	0.59	0.54
Y32A	0.02	0.02	0.12
Y33A	0.01	0	0.01
H34A	0.46	0.5	0.68
W35A	0.04	0.06	0.07
N35aA	0.98	0.85	1.06
CDRH2			
N50A	0.74	1.02	1.07
I51A	1.28	1.16	1.22
D52A	1.12	1.34	1.16
G52aA	0.76	0.83	0.79
N53A	1.03	1.09	1
S54A	1.13	1.08	0.95
S56A	1.1	1.26	1.21
T57A	1.06	1.18	1.17
N58A	0.75	1.3	1.35
Y59A	1.27	1.26	1.23
N60A	1.26	1.21	1.26
P61A	1.3	1.2	1.22
S62A	1.12	1.16	1.1
L63A	1.1	1.15	1.2
K64A	1.05	1	1.14
T65A	1.1	1	1.07

Mutations	Binding affinity relative to WT EBOV GPΔMuc	SUDV GPΔMuc	BDBV GPΔTM
CDRH3			
D95A	0	0	0
P96A	0.73	0.91	0.74
G97A	0.26	0.79	0.93
F98A	0.43	0.52	0.81
T99A	0.32	0.35	0.71
I100A	0.11	0.31	0.38
F100aA	0.01	0	0.01
G100bA	0.64	0.74	0.8
V100cA	0.57	0.91	1.14
V100dA	0.39	0.5	0.57
I100eA	0.07	0.18	0.22
T100fA	1.1	0.97	0.84
S100gA	1.13	0.96	0.94
W100hA	0.25	0.3	0.33
S100iA	0.62	0.95	1.18
G100jA	0.61	0.66	0.56
L100kA	0.85	1.09	0.87
D101A	0.02	0.48	0
S102A	1.17	1.06	0.89

[a]WT affinity is defined as the value of 1
[b]CDRs are defined by Kabat system
Relative affinity < 0.33 (3-fold decrease) is highlighted

Mutations	Binding affinity relative to WT EBOV GPΔMuc	SUDV GPΔMuc	BDBV GPΔTM
CDRL1			
R24A	1.04	1.05	0.92
S26A	1.04	0.99	0.85
Q27A	1.11	1.05	1.06
S28A	1.03	1.13	0.99
I29A	1.1	1.17	0.97
S30A	1.15	1.13	1
N31A	1.07	1.14	1.04
N32A	1.14	1.15	1.04
L33A	1.05	1.1	1.08
CDRL2			
S52A	1.15	0.99	0.87
N53A	0.89	0.93	0.71
L54A	1.08	0.99	0.77
S56A	1.07	0.98	0.91
CDRL3			
Q89A	0.9	0.95	0.66
Q90A	1.13	1.03	0.93
H91A	0.96	1.04	0.8
N92A	0.85	1.04	0.79
T93A	1.1	1.16	0.95
L94A	1.03	1.18	0.95
P95A	0.6	1.03	0.68
L96A	1.11	1.03	0.85
T97A	1.03	1.18	0.87

D

	Ebolavirus Glycoproteins											
	EBOV GPΔMuc			EBOV GP_{CL}			SUDV GPΔMuc			BDBV GPΔTM		
Antibody	$K_{D\,(nM)}$	$k_{on\,(1/Ms)}$	$k_{off\,(1/s)}$	$K_{D\,(nM)}$	$k_{on\,(1/Ms)}$	$k_{off\,(1/s)}$	$K_{D\,(nM)}$	$k_{on\,(1/Ms)}$	$k_{off\,(1/s)}$	$K_{D\,(nM)}$	$k_{on\,(1/Ms)}$	$k_{off\,(1/s)}$
CA45	3.2	3.5×10^4	1.1×10^{-4}	< 0.001	1.6×10^5	$< 1.0 \times 10^{-7}$	1.8	9.7×10^4	1.8×10^{-4}	1.2	2.8×10^4	3.3×10^{-5}
CA45-$H_{GL}L_{GL}$	3100	2.0×10^2	6.3×10^{-4}	< 0.001	7.7×10^4	$< 1.0 \times 10^{-7}$	887	5.6×10^2	4.9×10^{-4}	NB	-	-
CA45-$H_{m}L_{GL}$	6.9	1.9×10^4	1.3×10^{-4}	< 0.001	1.2×10^5	$< 1.0 \times 10^{-7}$	24	6.1×10^4	1.4×10^{-3}	43	1.3×10^4	5.8×10^{-4}

Figure 4

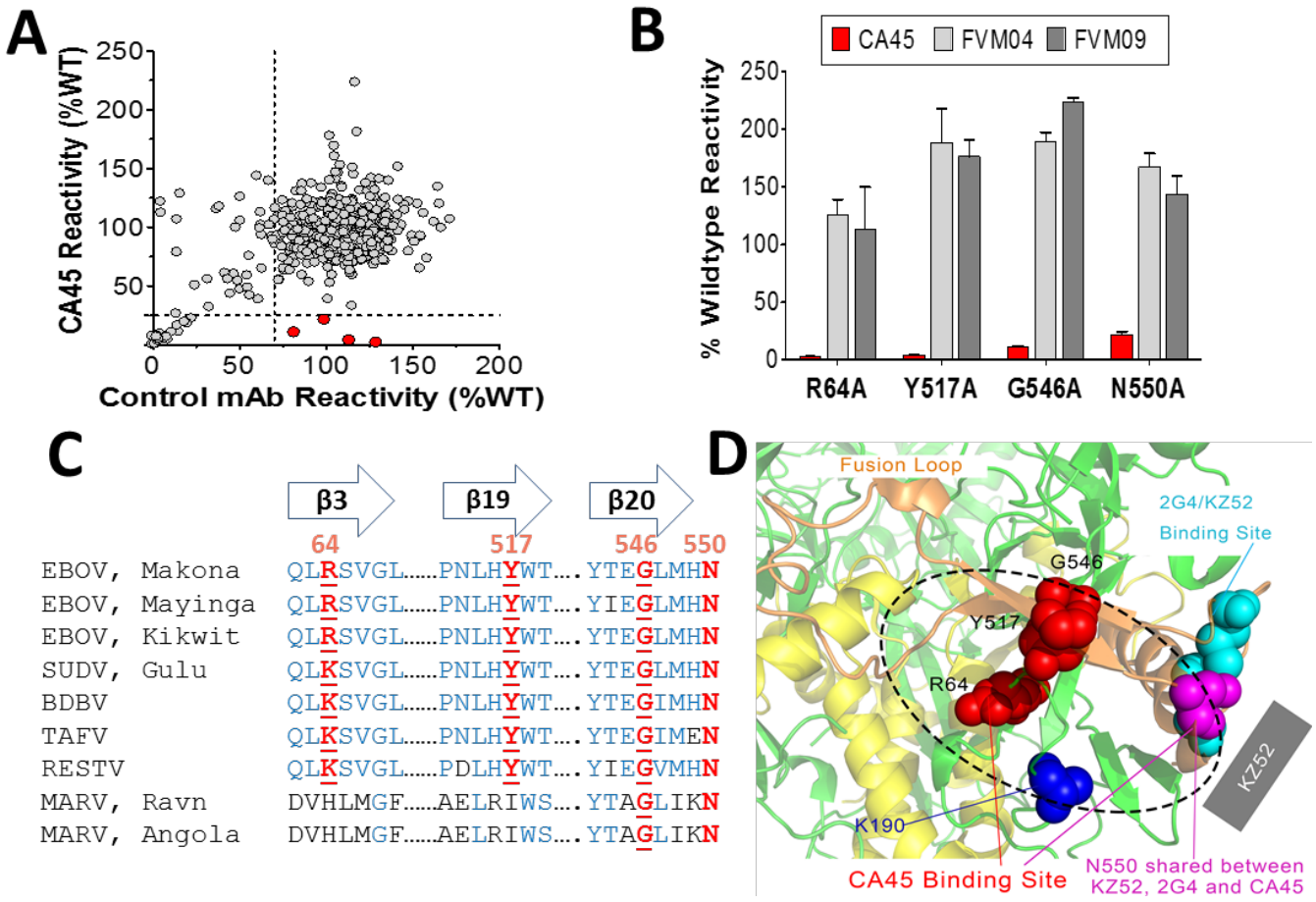
A
CA45 Reactivity (%WT)
Control mAb Reactivity (%WT)
B
CA45
FVM04
FVM09
% Wildtype Reactivity
R64A
Y517A
G546A
N550A
C
β3
β19
β20
64
517
546
550
EBOV, Makona
EBOV, Mayinga
EBOV, Kikwit
SUDV, Gulu
BDBV
TAFV
RESTV
MARV, Ravn
MARV, Angola
D
Fusion Loop
2G4/KZ52
Binding Site
G546
Y517
R64
K190
KZ52
CA45 Binding Site
N550 shared between
KZ52, 2G4 and CA45

Figure 5

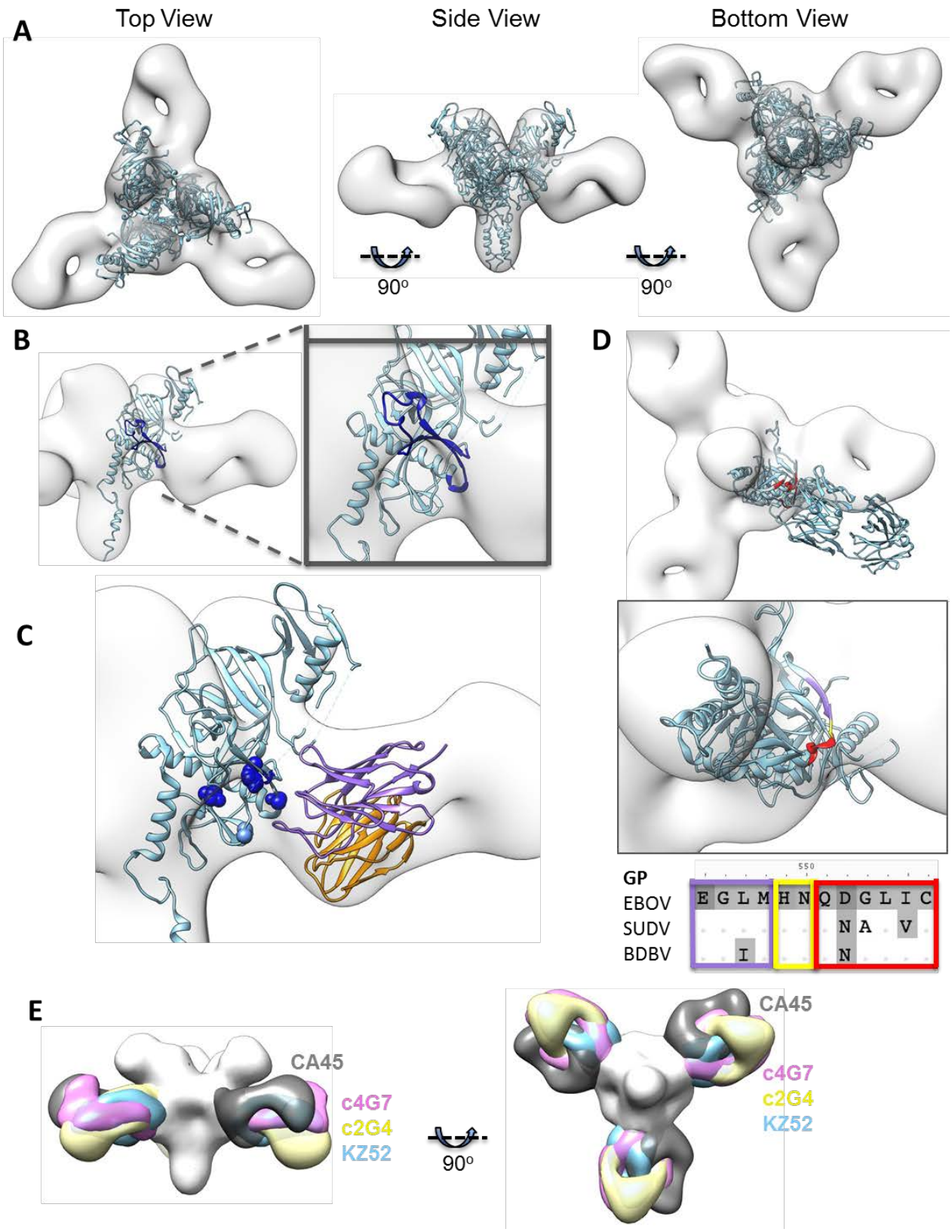
A
Top View
Side View
Bottom View
90°
90°
B
C
D
GP
EBOV
SUDV
BDBV
550
E G L M H N Q D G L I C
N A V
I
N
E
CA45
c4G7
c2G4
KZ52
90°
CA45
c4G7
c2G4
KZ52

Figure 6

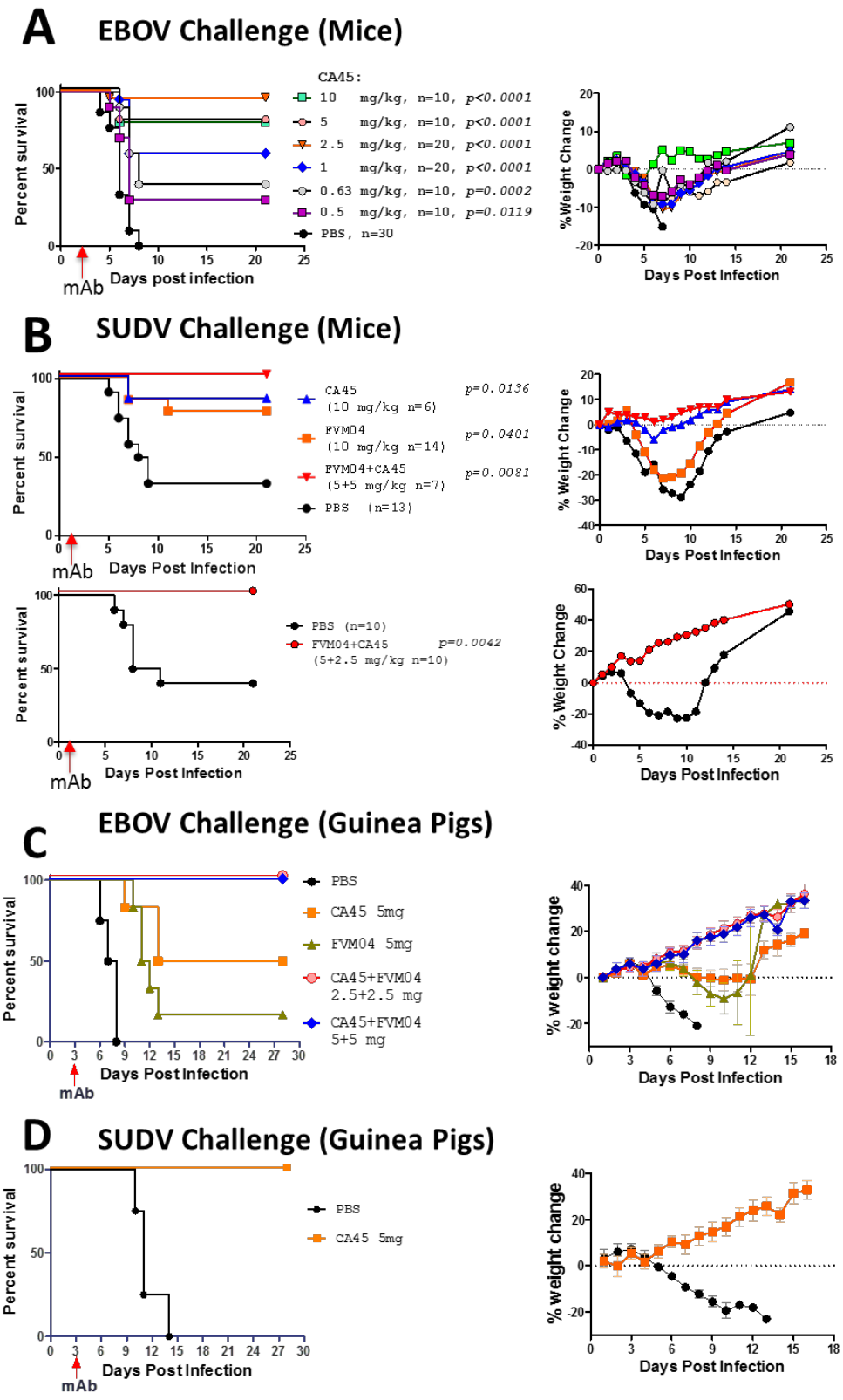
A
EBOV Challenge (Mice)
CA45:
10 mg/kg, n=10, p<0.0001
5 mg/kg, n=10, p<0.0001
2.5 mg/kg, n=20, p<0.0001
1 mg/kg, n=20, p<0.0001
0.63 mg/kg, n=10, p=0.0002
0.5 mg/kg, n=10, p=0.0119
PBS, n=30
Percent survival
Days post infection
mAb
% Weight Change
Days Post Infection
B
SUDV Challenge (Mice)
CA45 (10 mg/kg n=6) p=0.0136
FVM04 (10 mg/kg n=14) p=0.0401
FVM04+CA45 (5+5 mg/kg n=7) p=0.0081
PBS (n=13)
PBS (n=10)
FVM04+CA45 (5+2.5 mg/kg n=10) p=0.0042
C
EBOV Challenge (Guinea Pigs)
PBS
CA45 5mg
FVM04 5mg
CA45+FVM04 2.5+2.5 mg
CA45+FVM04 5+5 mg
% weight change
D
SUDV Challenge (Guinea Pigs)

Figure 7

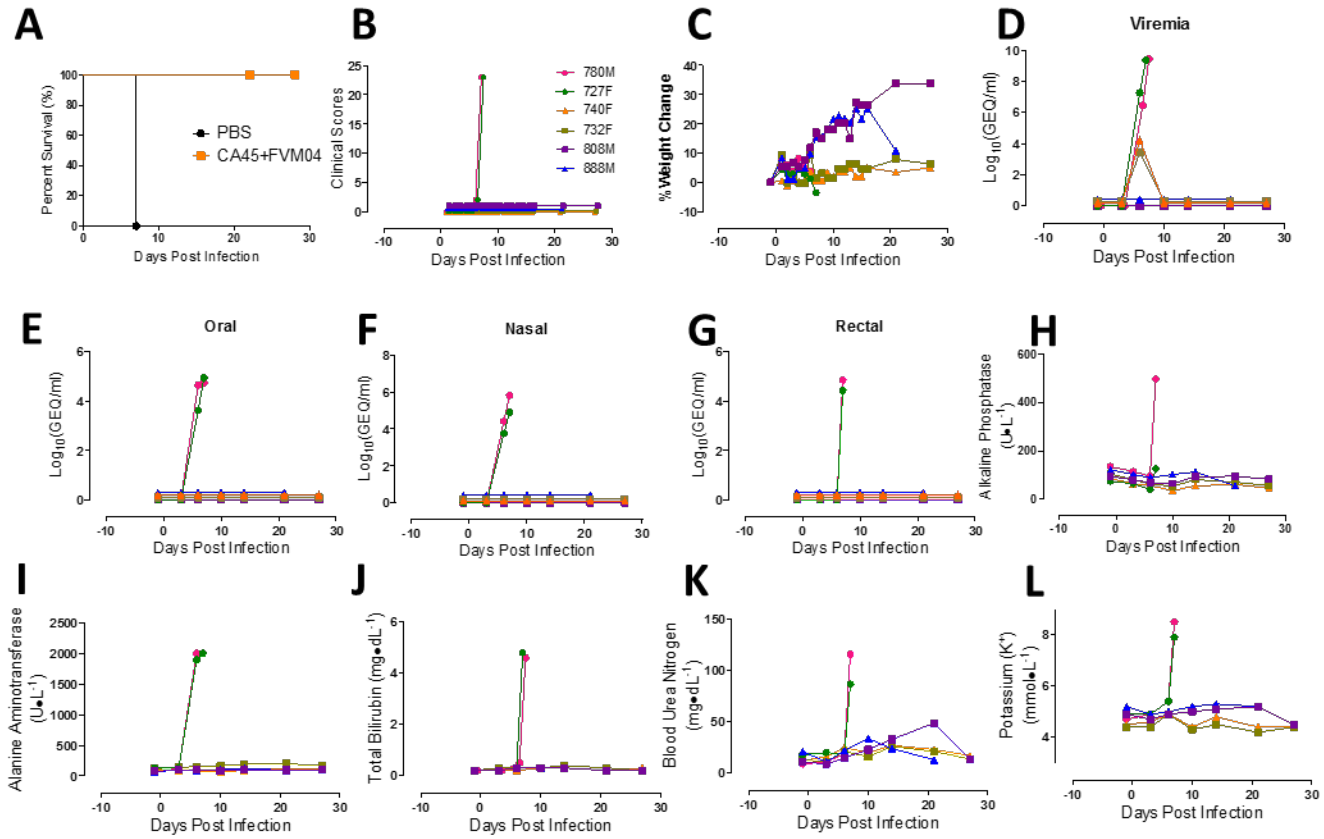
A
Percent Survival (%)
PBS
CA45+FVM04
Days Post Infection
B
Clinical Scores
780M
727F
740F
732F
808M
888M
Days Post Infection
C
% Weight Change
Days Post Infection
D
Viremia
Log10(GEQ/ml)
Days Post Infection
E
Oral
Log10(GEQ/ml)
Days Post Infection
F
Nasal
Log10(GEQ/ml)
Days Post Infection
G
Rectal
Log10(GEQ/ml)
Days Post Infection
H
Alkaline Phosphatase (U•L-1)
Days Post Infection
I
Alanine Aminotransferase (U•L-1)
Days Post Infection
J
Total Bilirubin (mg•dL-1)
Days Post Infection
K
Blood Urea Nitrogen (mg•dL-1)
Days Post Infection
L
Potassium (K+) (mmol•L-1)
Days Post Infection

Supplemental Information

Table S1. Properties of the GP-specific clones isolated by flow cytometric sorting. *Related to Main Figure 1*.

Animal	**Cyno. 20667**
Immunization time point	day 84 (28 days after the 3rd immunization)
Probe	Insect-expressed Ebola /mammalian-expressed Sudan GPΔmuc
Total PBMC	6,710,000
Total Memory B cell CD20+IgG+IgM-CD27+	111,408
Total Memory B cell %	1.7
Total GP-specific Memory B cell EBOV or SUDV_GP+ CD20+IgG+IgM-CD27+(EBOV or SUDV) GP+	530
GP-specific Memory B cell %	0.5
Total cross-reactive Memory B cell EBOV & SUDV_GP+ CD20+IgG+IgM-CD27+ (EBOV & SUDV) GP+	68
GP Cross-reactive Memory B cell %	0.06
Sorted cells	29
Sorted cells with VH or VL amplified	27
Sorted cells with paired VH and VL	17
Expressed mAbs	12
GP+ mAbs	11
Sorting precision ((GP+mAbs/Expressed mAbs)*100)	92%

Table S2. GP-specific mAb binding specificity validation and virus neutralization capacity (pseudotype virus assay). *Related to Main Figure 1*.

mAb	Related clones	ELISA binding		Neutralization	
		EBOV GPΔmuc	SUDV GPΔmuc	EBOV	SUDV
CA39	CA48, FVM04 [a]	++	++	moderate	-
CA40	FVM08 & FVM21[a]	+++	+++	-	-
CA41	Single expansion [b]	+	+	-	-
CA42	FVM22 & FVM09 [a]	+++	+++	moderate	-
CA44	Single expansion [b]	+++	+++	-	-
CA45	Single expansion [b]	+++	+++	+	+
CA46	CA51	-	-	-	-
CA48	CA39, & FVM04 [a]	+++	+++	-	-
CA49	Single expansion [b]	++	+	-	-
CA54	Single expansion [b]	+	++	moderate	-
CA57	Single expansion [b]	+	+	-	-
CA58	Single expansion [b]	+++	+++	-	-
KZ52 (control)		+++	-	+	-

[a] Previously published Ebola GP-specific mAb (Keck et al., 2016, J.Virol., 90:279-291)

[b] Isolated as single clone in this sorting experiment

ELISA binding: +++: OD450max= 2.0-3.0; ++: OD450max=1.0-2.0; +: OD450max=0.3-1.0; -: OD450max <0.3

Neutralization: -: IC_{50} > 50 µg/mL; +: IC_{50}< 50 µg/mL; Moderate: IC_{50}=50 µg/mL

Table S3. Genetic analysis of CA45 heavy- and light- chain variable region by IgBlast program. *Related to Main Figure 3*.

mAb	V gene	D gene	J gene	CDR3(#aa)[a]	V gene mutation	
					Nucleotide (nt)	Amino acid (aa)
CA45 heavy chain	VH4-21	IGHD3-4	IGHJ6-1	19	9.6% (29/302)	14% (14/100)
CA45 light chain	IGKV1-5		IGKJ6	9	7.5% (21/280)	13.9% (13/93)

[a]CDR3 length was determined based on the Kabat numbering

Table S4: ELISA based Competition of mAbs with CA45 for EBOVGPΔTM Binding. (A) CA45 was combined with other well characterized mAbs KZ52, 13C6, FVM04, FVM02 and FVM09 in a competition matrix. EBOV GPΔTM was coated on 96-well plates and a saturating concentration of mAb1 was added for 30 min before adding mAb2-biotin at its pre-determined EC_{50} µg/mL. mAb2-biotin binding was detected with anti-streptavidin-HRP and percent competition was compared to a control antibody. *Related to Main Figure 4*.

		2nd Mab					
		CA45	**KZ52**	**13C6**	**FVM04**	**FVM02**	**FVM09**
1st MAb	**CA45**	83.9	69.2	2.5	15.5	-1.1	18
	KZ52	86.8	79.8	9.5	12.9	NT	NT
	13C6	19.1	23	92.2	101.9	NT	NT
	FVM04	9.9	19.1	83.6	100.3	9.3	3.8

Figure S1: CA45 does not inhibit receptor binding or initial triggering of membrane fusion but partially inhibits cleavage of GP. (A) FVM04 but not CA45, KZ52, or MR72 inhibit the interaction of GP_{CL} with NPC-1 domain C (dC) determined in an ELISA based assay. (B) CA45 partially blocks the cleavage of GP → GP_{CL} determined in vitro by using thermolysin. GP, partially cleaved GP, and completely cleaved GP (GP_{CL}) were detected by Western blot using a monoclonal antibody specific for the core GP1 (mAb21D10). (C) Lipid mixing of viral and endosomal membranes is inhibited by NH_4Cl, KZ52 (100 mg/mL) but not CA45 (100 mg/mL) as determined by measuring viral dequenching using an live cell imaging assay. *Related to Main Figure 2.*

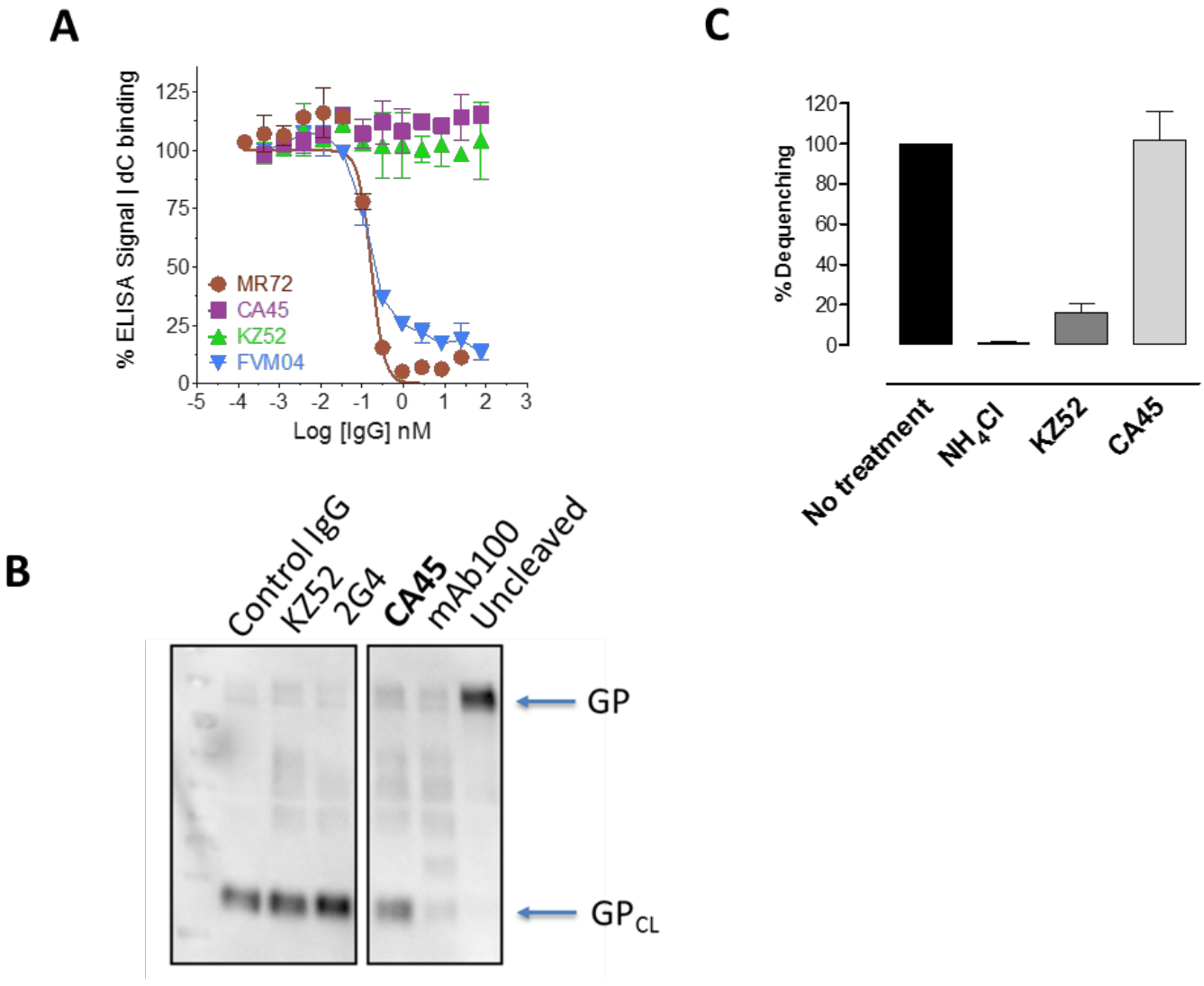

Fig. S2. Alanine scanning analysis of CA45. Alanine scanning mutants of CA45 heavy (HC, upper) and light chain (LC, lower) CDR loops were assessed for binding affinity for (A) SUDV and (B) BDBV GPΔmuc relative to the wildtype (WT) IgG molecule. Mutated residues with relative binding signal < 0.33 (with relative affinity decreases more than 3-folds) were considered to be critical for EBOV GP binding. *Related to Main Figure 3*.

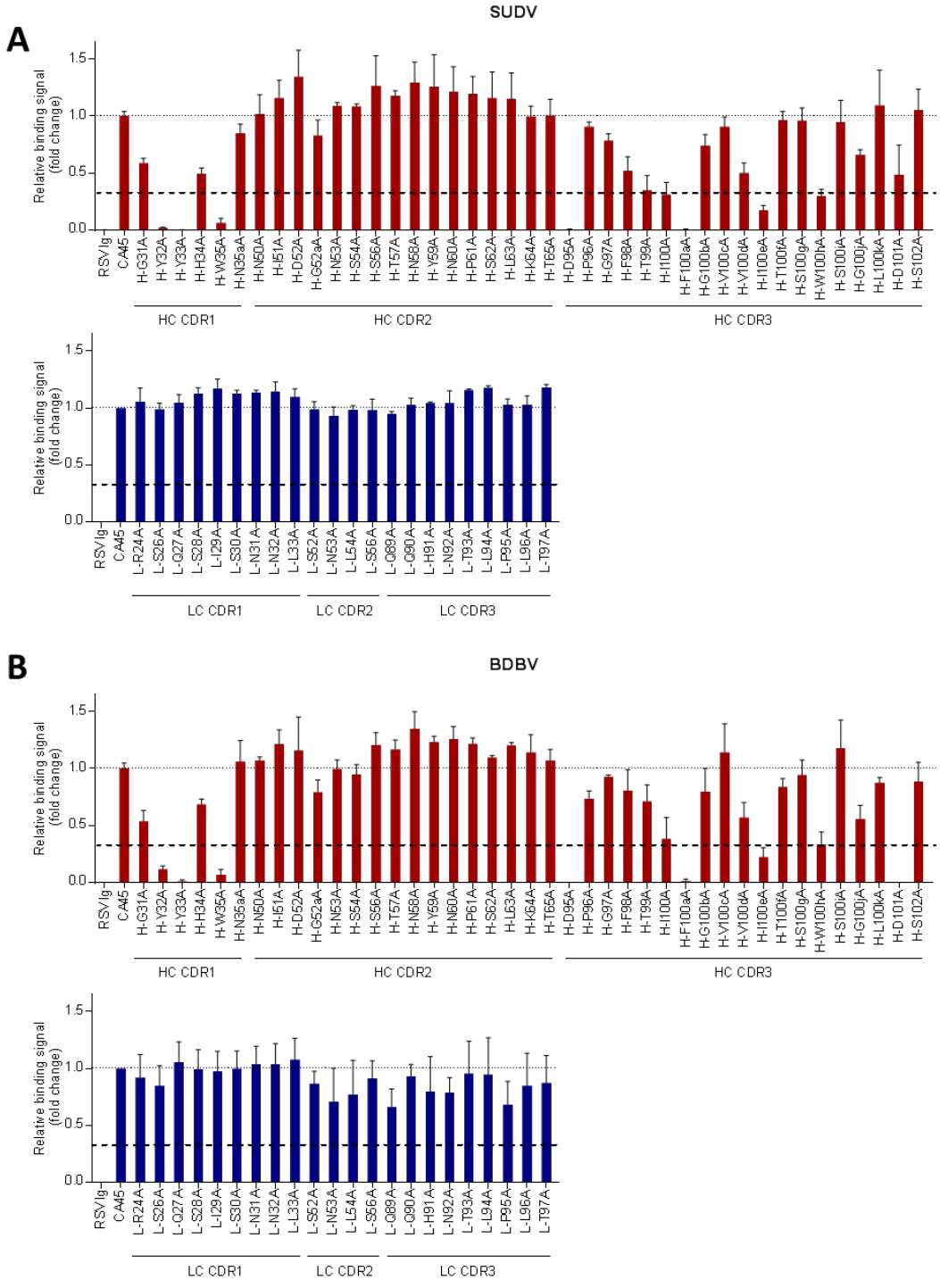

Fig. S3. Characterization of the binding properties of germline reverted CA45. A-K: Kinetic Analysis of CA45, CA45 $H_{GL}L_{GL}$ and CA45 H_mL_{GL}. The sensograms show the association and dissociation of mature CA45 (top row), CA45 $H_{GL}L_{GL}$ (middle row) and CA45 H_mL_{GL} (bottom row) to EBOV GPΔMuc (A, E, H), EBOV GP_{CL} (B,F,I), SUDV GPΔMuc (C,G,J) and BDBV GPΔTM (D,K). Concentrations analyzed are indicated (colored) and data was fit to a 1:1: binding model (red dashes).

L-N: Pseudotype Neutralization by CA45. Mature CA45 (blue), CA-H_mL_{GL} (green), or CA45-$H_{GL}L_{GL}$ (orange) was pre-incubated with VSV-EBOV-GP-Luc, VSV-SUDV-GP-Luc or VSV-BDBV-GP-Luc for 1 hour before the addition to vero cells. Luciferase activity was measured 24 hours later and percent neutralization was calculated based on untreated wells containing virus only. Data was analyzed on Prism GraphPad and fit to a 4PL curve to obtain EC_{50}. *Related to Main Figure 3.*

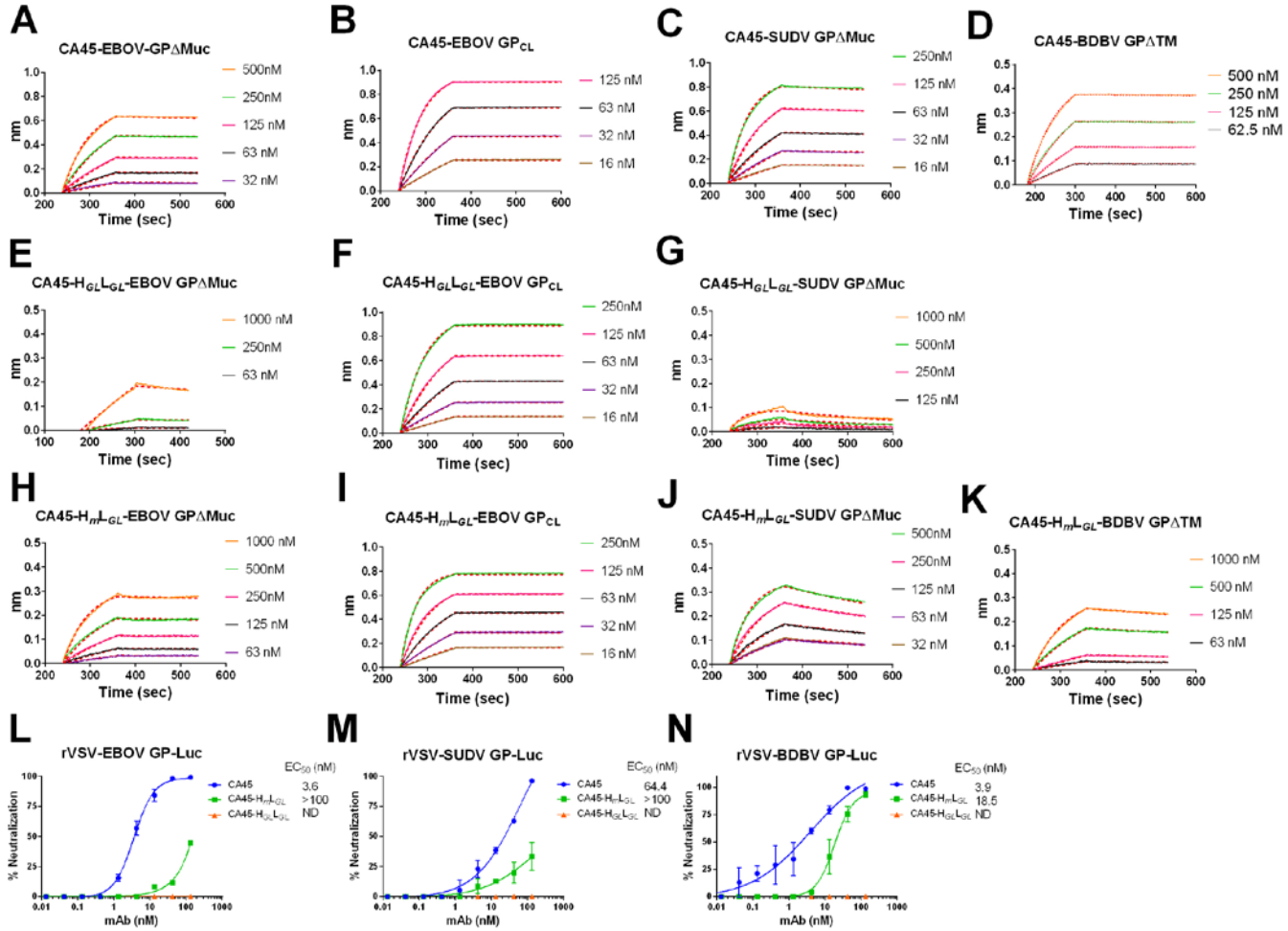

Figure. S4: The environment of CA45 epitope in EBOV GP versus cleaved GP and occlusion of the epitope by the DFF lid. (A) Overlay of EBOV GPΔmuc (PDB: 5JQ3, green) and GP_{CL} (PDB: 5HJ3, blue). The DFF lid (D192, F192, F193) shown in yellow in GPDmuc is disordered and untraceable in GP_{CL} structure. (B) The structure of EBOV GP bound to toremifene (cyan) (PDB: 5JQ7) with displaced and disordered DFF lid and dispositioned K191 (compared to A). (C) CA45 shows enhanced binding to each of single alanine substitutions within the DFF lid compared to we GP. *Related to Main Figure 4*.

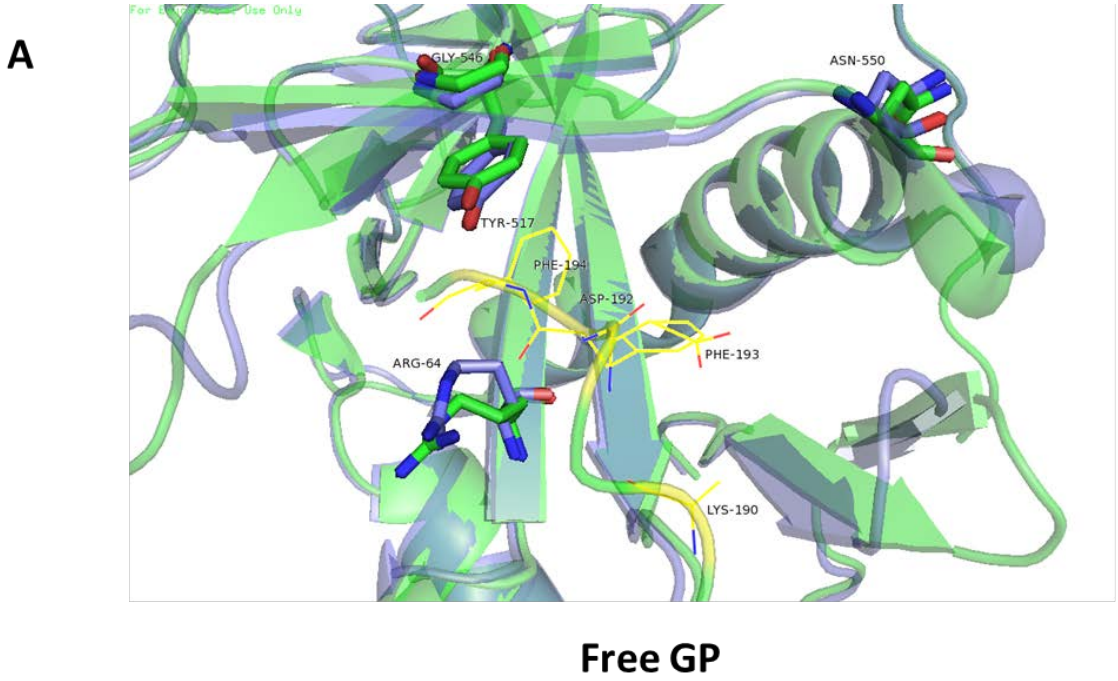

Figure S5: CA45 escape mutants. Four rounds of selection were performed by growing VSV-EBOV GP in presence of CA45 and virus from 4th passage was plaque purified and 10 clones sequenced. (A) position of identified mutations in 10 CA45 resistant clones. (B) Position of the two mutations shared among all resistant clones in the structure of EBOV GPΔmuc (5JQ3). (C) loss of binding of CA45 to the resistant clones determined by ELISA. (D) Loss of CA45 neutralizing activity towards the resistant clones. (E) Individual mutations in the escape sites do not affect CA45 binding indicating that combined mutation is needed for escape. (F) neutralization of CA45 escape mutants by FVM04. *Related to Main Figure 4*.

A

Plaque #	Mutation		
1	A101V	K588R	
2	A101V	K588R	N643D
3	A101V	K588R	
4	A101V	K588R	
5	A101V	K588R	
6	A101V	K588R	
7	A101V	K588R	
8	A101V	K588R	
9	A101V	K588R	
10	A101V	K588R	A654T

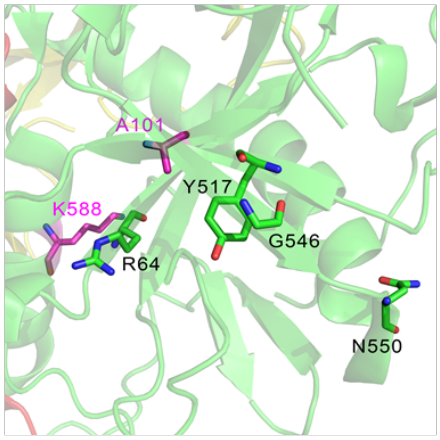

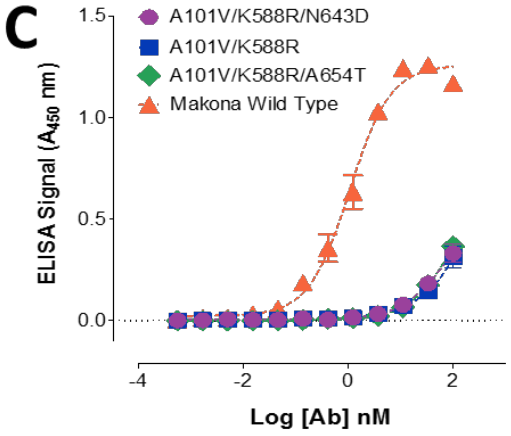

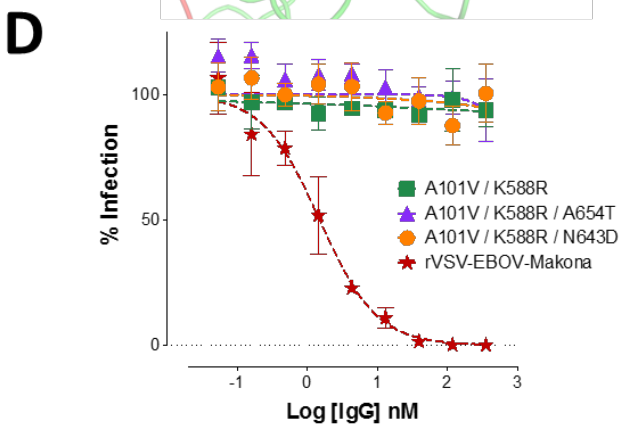

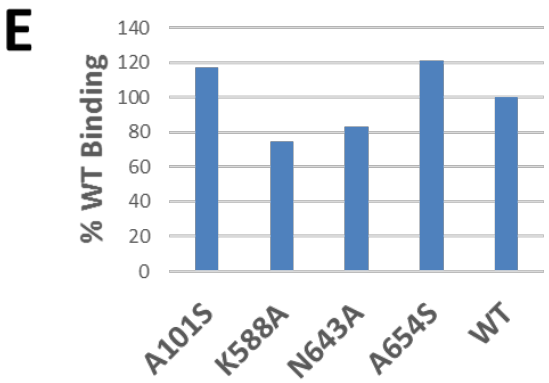

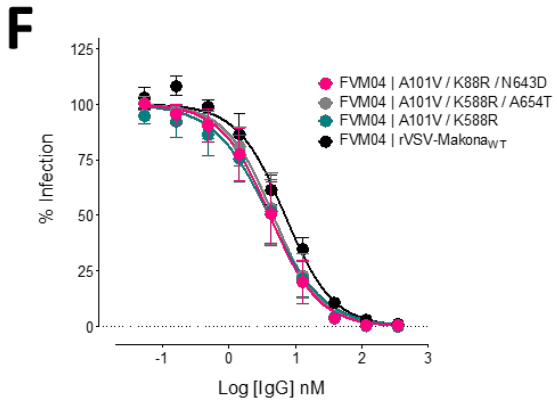

Figure S6: **Single-particle electron microscopy (EM) raw data of CA45 Fab bound to EBOV GPΔMuc**. Left, Raw micrograph of CA45 in complex with EBOV GPΔMuc; Middle, 2D classes of complex; Right, the FSC curve showing the 3D reconstruction at 11 Å. *Related to Main Figure 5*.

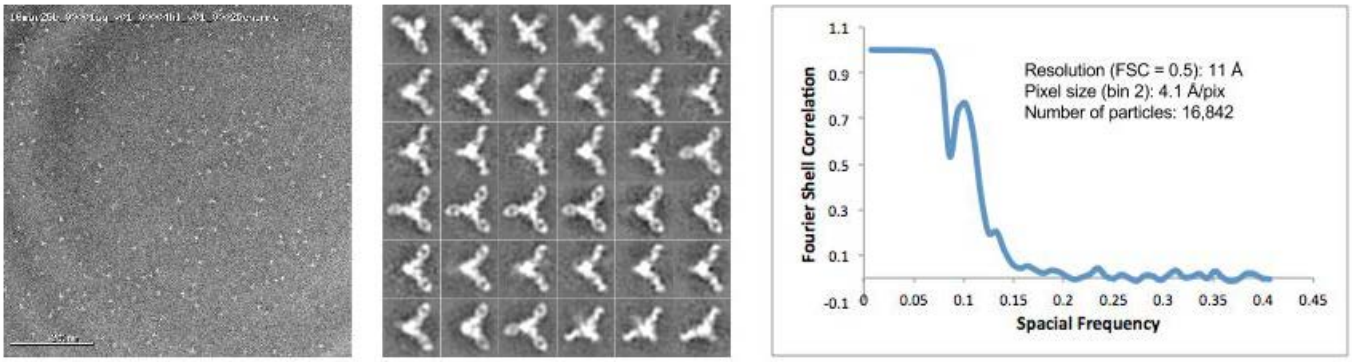

Figure S7: Hematological and blood chemistry changes in ferrets treated a cocktail of CA45 and FVM04 or PBS as controls (animals 780M and 727F). *Related to Main Figure 7*.

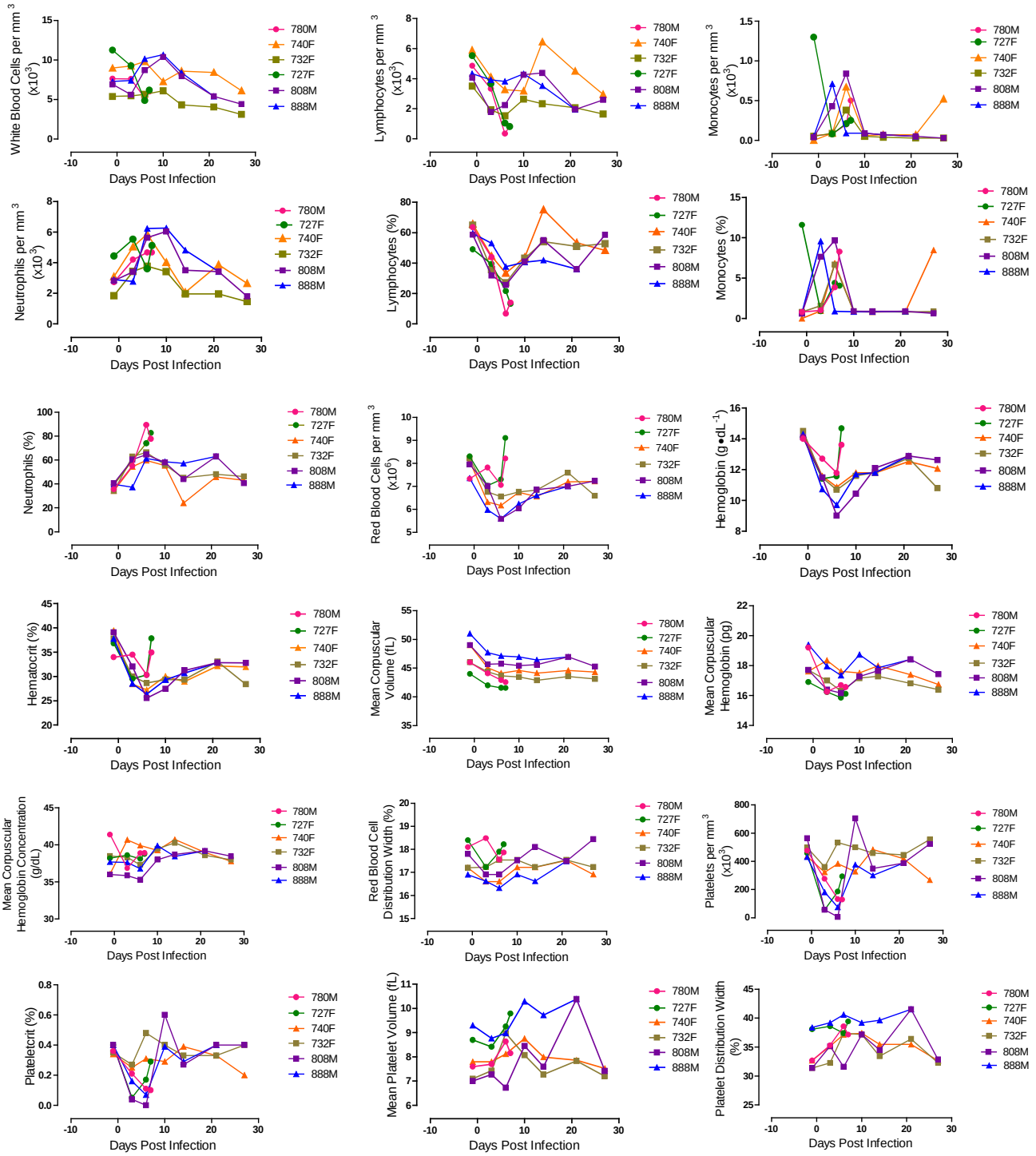

Figure S7, Continued

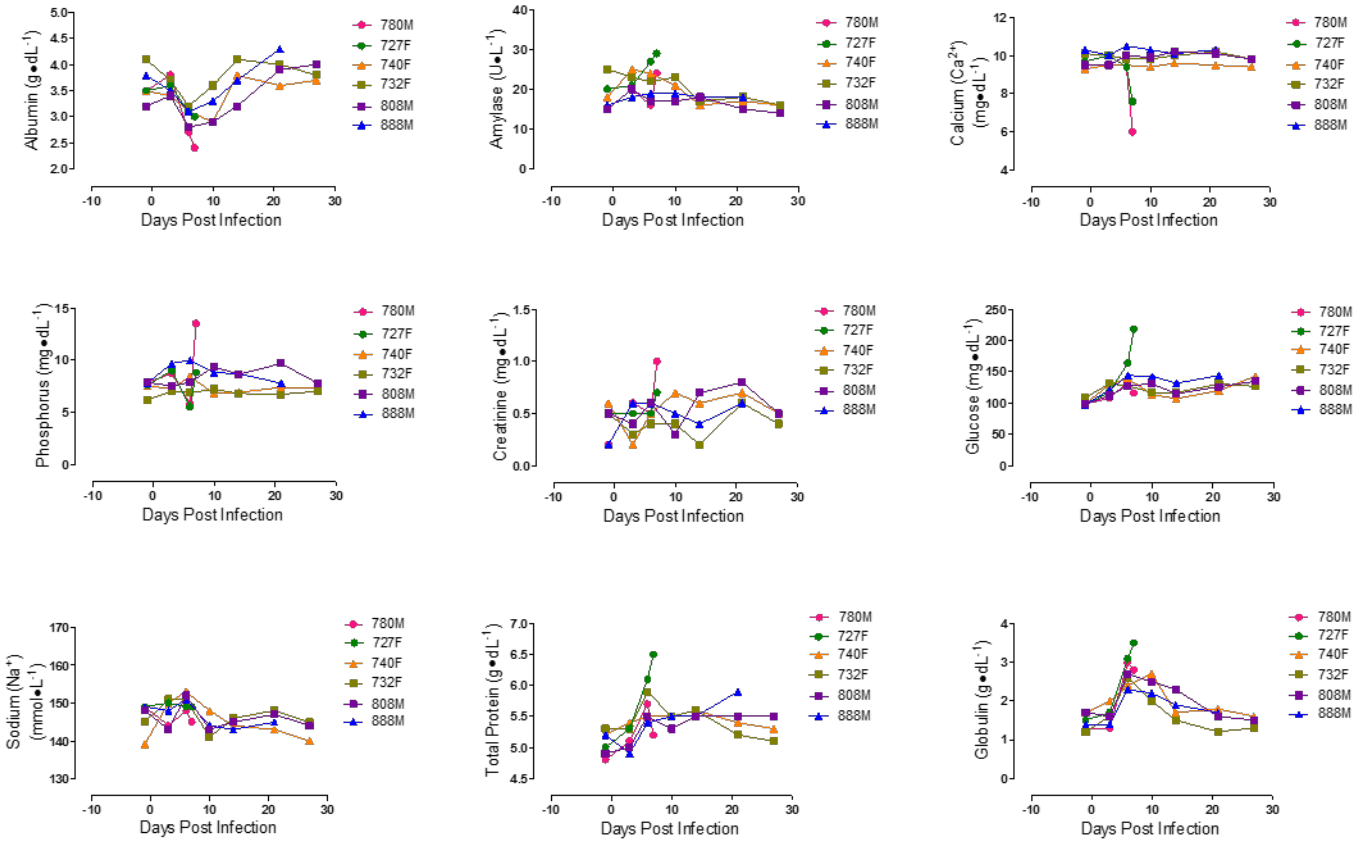

Figure 1. Discovery of CA45

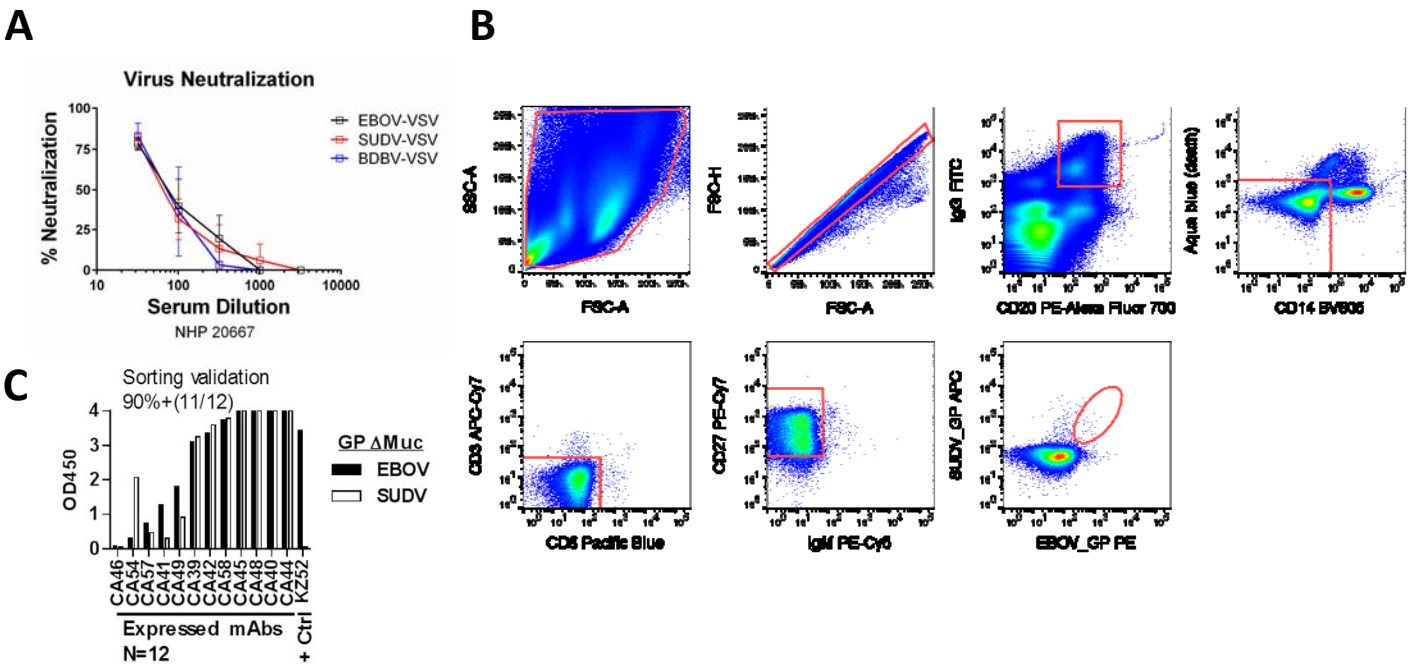

Fig. 2

A ELISA Binding

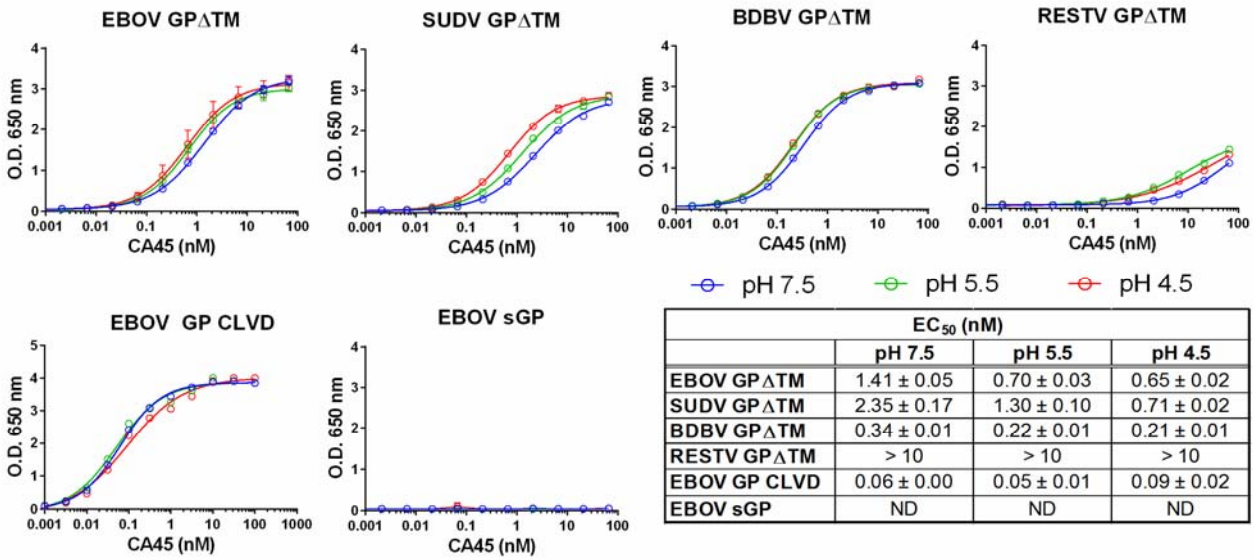

	EC$_{50}$ (nM)		
	pH 7.5	pH 5.5	pH 4.5
EBOV GPΔTM	1.41 ± 0.05	0.70 ± 0.03	0.65 ± 0.02
SUDV GPΔTM	2.35 ± 0.17	1.30 ± 0.10	0.71 ± 0.02
BDBV GPΔTM	0.34 ± 0.01	0.22 ± 0.01	0.21 ± 0.01
RESTV GPΔTM	> 10	> 10	> 10
EBOV GP CLVD	0.06 ± 0.00	0.05 ± 0.01	0.09 ± 0.02
EBOV sGP	ND	ND	ND

B Binding Kinetics

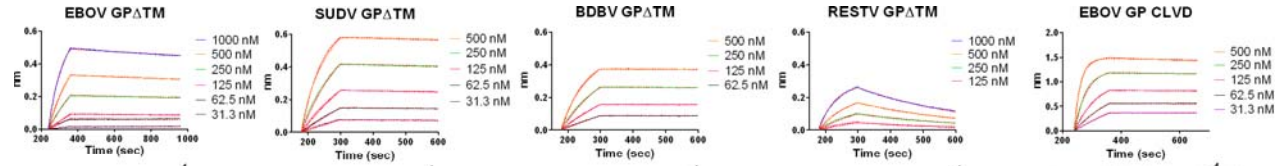

EBOV GPΔTM	SUDV GPΔTM	BDBV GPΔTM	RESTV GPΔTM	EBOV GP CLVD
k_{on} = (1.3 ± 0.1) x 10^4 /M sec	k_{on} = (3.1 ± 0.1) x 10^4 /M sec	k_{on} = (2.8 ± 0.1) x 10^4 /M sec	k_{on} = (1.7 ± 0.1) x 10^4 /M sec	k_{on} = (1.6 ± 0.1) x 10^4 /M sec
k_{off} = (1.4 ± 0.1) x 10^{-4} /sec	k_{off} = (1.0± 0.1) x 10^{-4} /sec	k_{off} = (3.3 ± 0.4) x 10^{-5} /sec	k_{off} = (2.8 ± 0.1) x 10^{-3} /sec	k_{off} = < 1.0 x 10^{-7}/sec
K_D = 10.6 ± 0.1 nM	K_D = 3.3 ± 0.1 nM	K_D = 1.2 ± 0.1 nM	K_D = 161 ± 0.1 nM	K_D = < 6.3 pM
R^2 = 0.9997	R^2 = 0.9999	R^2 = 0.9999	R^2 = 0.9965	R^2 = 0.9997

C Neutralization

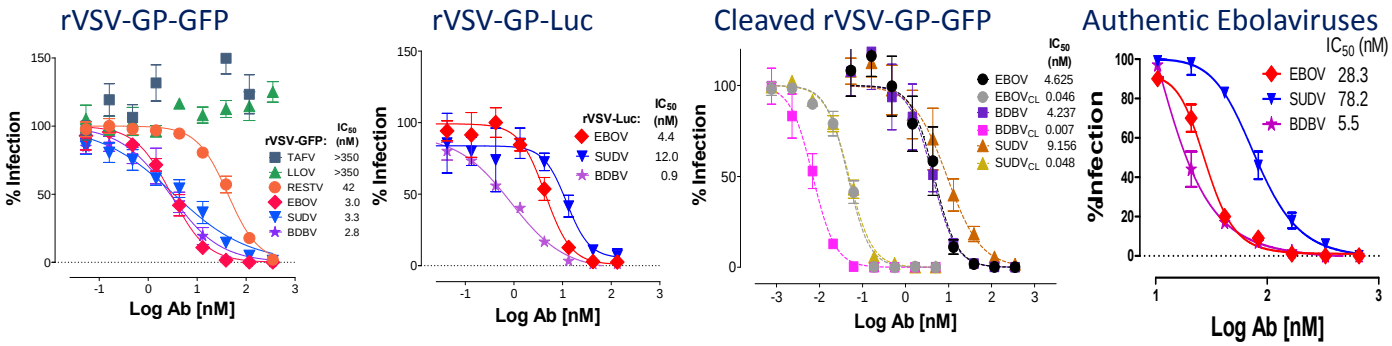

Fig. 3 CA45 genetics and mutagenesis

A

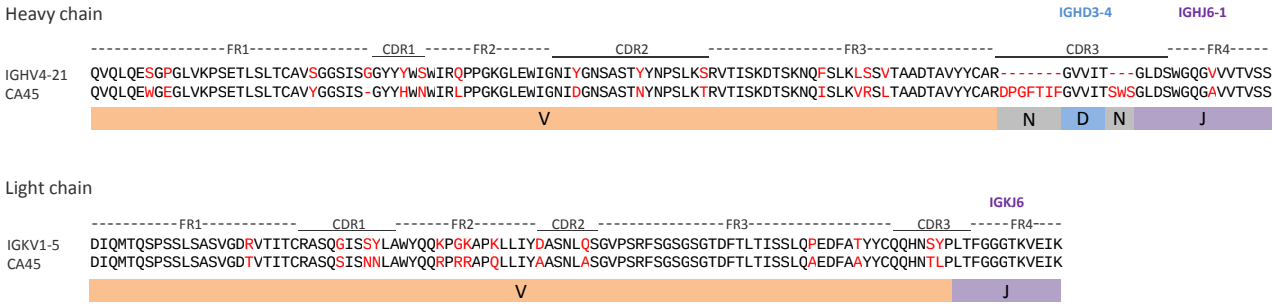

B

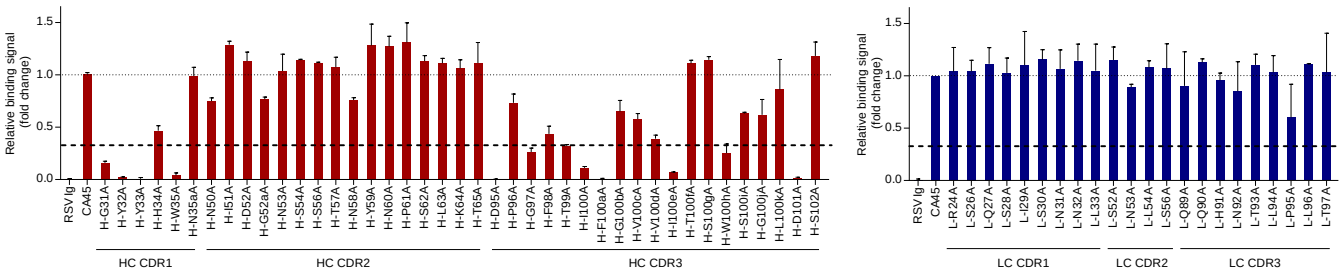

C

Mutations	Binding affinity relative to WT[a] EBOV GPΔMuc	SUDV GPΔMuc	BDBV GPΔTM
CDRH1[b]			
G31A	0.16	0.59	0.54
Y32A	0.02	0.02	0.12
Y33A	0.01	0	0.01
H34A	0.46	0.5	0.68
W35A	0.04	0.06	0.07
N35aA	0.98	0.85	1.06
CDRH2			
N50A	0.74	1.02	1.07
I51A	1.28	1.16	1.22
D52A	1.12	1.34	1.16
G52aA	0.76	0.83	0.79
N53A	1.03	1.09	1
S54A	1.13	1.08	0.95
S56A	1.1	1.26	1.21
T57A	1.06	1.18	1.17
N58A	0.75	1.3	1.35
Y59A	1.27	1.26	1.23
N60A	1.26	1.21	1.26
P61A	1.3	1.2	1.22
S62A	1.12	1.16	1.1
L63A	1.1	1.15	1.2
K64A	1.05	1	1.14
T65A	1.1	1	1.07

Mutations	Binding affinity relative to WT EBOV GPΔMuc	SUDV GPΔMuc	BDBV GPΔTM
CDRH3			
D95A	0	0	0
P96A	0.73	0.91	0.74
G97A	0.26	0.79	0.93
F98A	0.43	0.52	0.81
T99A	0.32	0.35	0.71
I100A	0.11	0.31	0.38
F100aA	0.01	0	0.01
G100bA	0.64	0.74	0.8
V100cA	0.57	0.91	1.14
V100dA	0.39	0.5	0.57
I100eA	0.07	0.18	0.22
T100fA	1.1	0.97	0.84
S100gA	1.13	0.96	0.94
W100hA	0.25	0.3	0.33
S100iA	0.62	0.95	1.18
G100jA	0.61	0.66	0.56
L100kA	0.85	1.09	0.87
D101A	0.02	0.48	0
S102A	1.17	1.06	0.89

[a]WT affinity is defined as the value of 1
[b]CDRs are defined by Kabat system
Relative affinity < 0.33 (3-fold decrease) is highlighted

Mutations	Binding affinity relative to WT EBOV GPΔMuc	SUDV GPΔMuc	BDBV GPΔTM
CDRL1			
R24A	1.04	1.05	0.92
S26A	1.04	0.99	0.85
Q27A	1.11	1.05	1.06
S28A	1.03	1.13	0.99
I29A	1.1	1.17	0.97
S30A	1.15	1.13	1
N31A	1.07	1.14	1.04
N32A	1.14	1.15	1.04
L33A	1.05	1.1	1.08
CDRL2			
S52A	1.15	0.99	0.87
N53A	0.89	0.93	0.71
L54A	1.08	0.99	0.77
S56A	1.07	0.98	0.91
CDRL3			
Q89A	0.9	0.95	0.66
Q90A	1.13	1.03	0.93
H91A	0.96	1.04	0.8
N92A	0.85	1.04	0.79
T93A	1.1	1.16	0.95
L94A	1.03	1.18	0.95
P95A	0.6	1.03	0.68
L96A	1.11	1.03	0.85
T97A	1.03	1.18	0.87

D

	Ebolavirus Glycoproteins											
	EBOV GPDMuc			EBOV GP_{CL}			SUDV GPDMuc			BDBV GPDTM		
Antibody	$K_{D\ (nM)}$	$k_{on\ (1/Ms)}$	$k_{off\ (1/s)}$	$K_{D\ (nM)}$	$k_{on\ (1/Ms)}$	$k_{off\ (1/s)}$	$K_{D\ (nM)}$	$k_{on\ (1/Ms)}$	$k_{off\ (1/s)}$	$K_{D\ (nM)}$	$k_{on\ (1/Ms)}$	$k_{off\ (1/s)}$
CA45	3.2	3.5×10^4	1.1×10^{-4}	<0.001	1.6×10^5	$< 1.0 \times 10^{-7}$	1.8	9.7×10^4	1.8×10^{-4}	1.2	2.8×10^4	3.3×10^{-5}
CA45-$H_{GL}L_{GL}$	3100	2.0×10^2	6.3×10^{-4}	<0.001	7.7×10^4	$< 1.0 \times 10^{-7}$	887	5.6×10^2	4.9×10^{-4}	NB[a]	-	-
CA45-H_mL_{GL}	6.9	1.9×10^4	1.3×10^{-4}	<0.001	1.2×10^5	$< 1.0 \times 10^{-7}$	24	6.1×10^4	1.4×10^{-3}	43	1.3×10^4	5.8×10^{-4}

Fig. 4

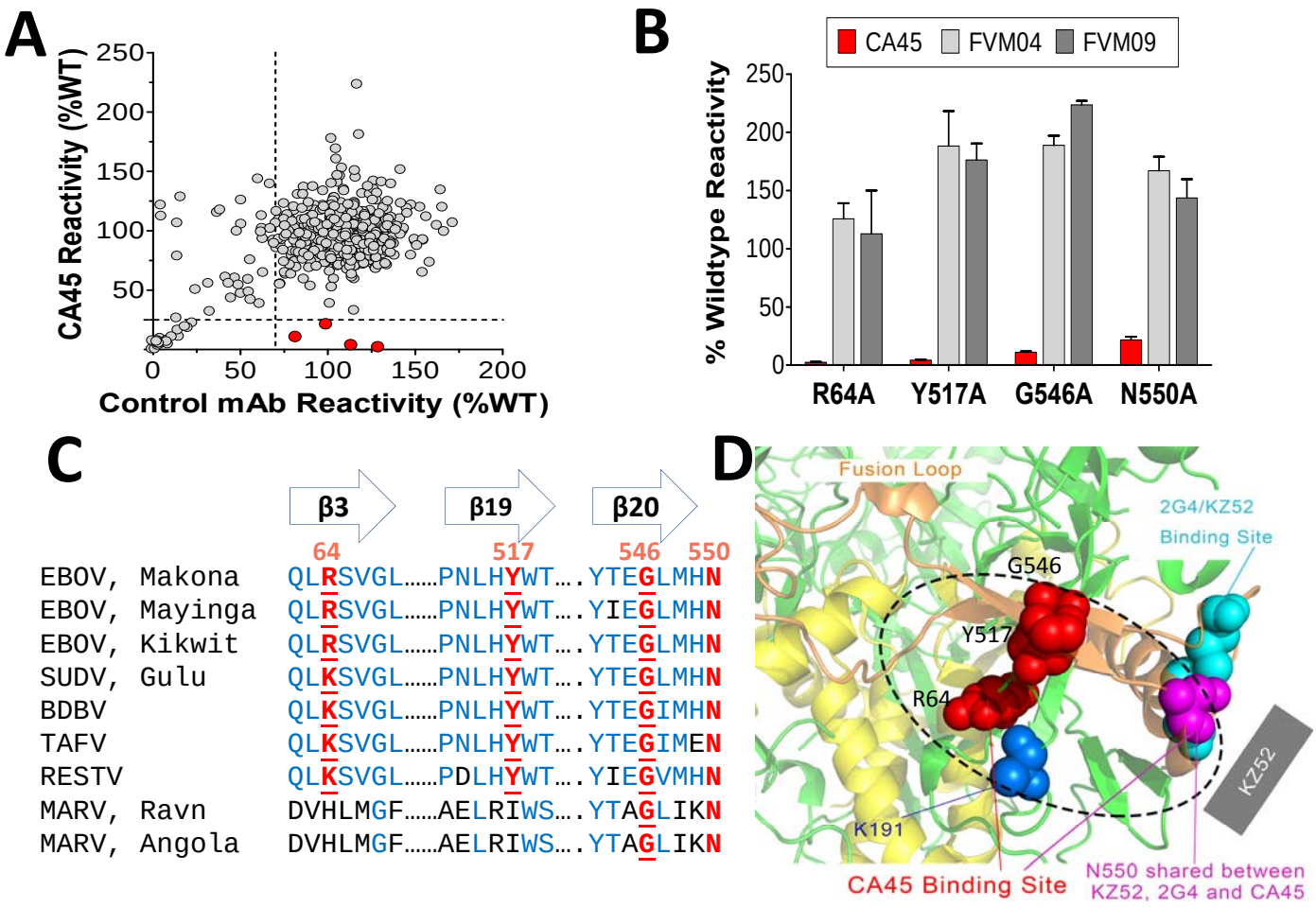
A
CA45 Reactivity (%WT)
Control mAb Reactivity (%WT)
B
CA45
FVM04
FVM09
% Wildtype Reactivity
R64A
Y517A
G546A
N550A
C
β3
β19
β20
64
517
546
550
EBOV, Makona QLRSVGL……PNLHYWT….YTEGLMHN
EBOV, Mayinga QLRSVGL……PNLHYWT….YIEGLMHN
EBOV, Kikwit QLRSVGL……PNLHYWT….YTEGLMHN
SUDV, Gulu QLKSVGL……PNLHYWT….YTEGLMHN
BDBV QLKSVGL……PNLHYWT….YTEGIMHN
TAFV QLKSVGL……PNLHYWT….YTEGIMEN
RESTV QLKSVGL……PDLHYWT….YIEGVMHN
MARV, Ravn DVHLMGF……AELRIWS….YTAGLIKN
MARV, Angola DVHLMGF……AELRIWS….YTAGLIKN
D
Fusion Loop
2G4/KZ52
Binding Site
G546
Y517
R64
K191
KZ52
CA45 Binding Site
N550 shared between
KZ52, 2G4 and CA45

Fig. 5 CA45 EM and approaching angle

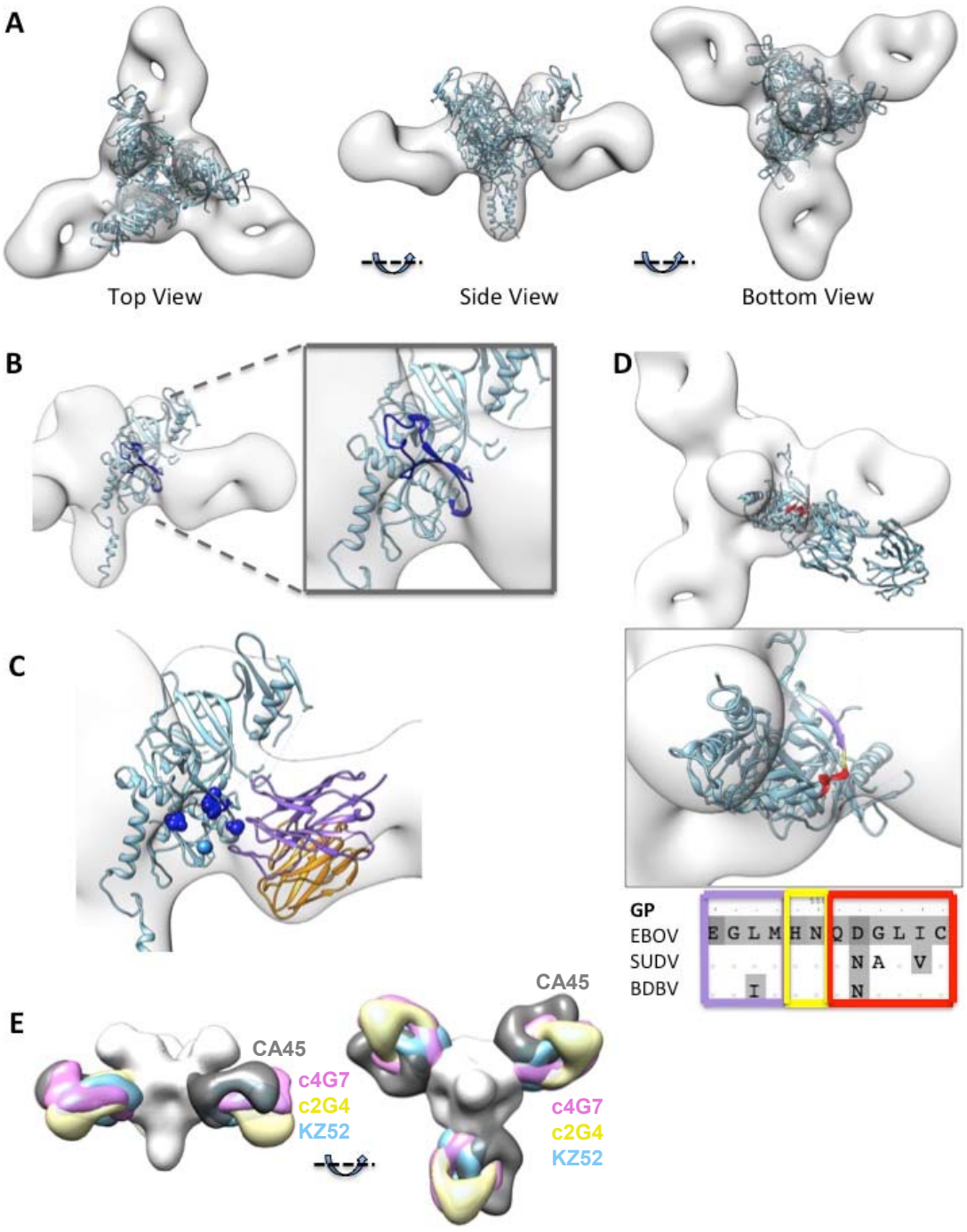

Fig. 6

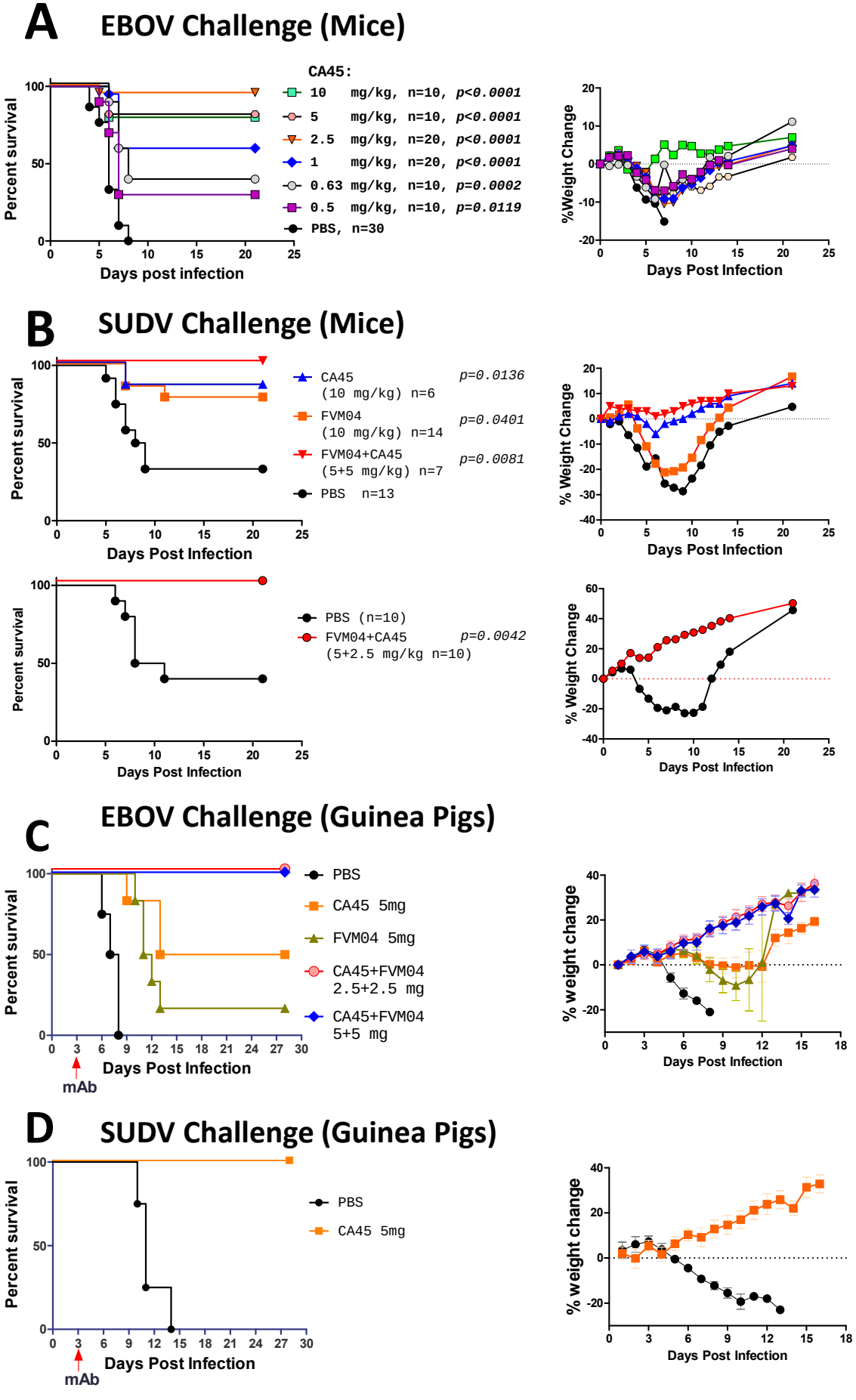
A
EBOV Challenge (Mice)
CA45:
10 mg/kg, n=10, p<0.0001
5 mg/kg, n=10, p<0.0001
2.5 mg/kg, n=20, p<0.0001
1 mg/kg, n=20, p<0.0001
0.63 mg/kg, n=10, p=0.0002
0.5 mg/kg, n=10, p=0.0119
PBS, n=30
Percent survival
Days post infection
%Weight Change
Days Post Infection
B
SUDV Challenge (Mice)
CA45 (10 mg/kg) n=6
p=0.0136
FVM04 (10 mg/kg) n=14
p=0.0401
FVM04+CA45 (5+5 mg/kg) n=7
p=0.0081
PBS n=13
PBS (n=10)
FVM04+CA45 (5+2.5 mg/kg n=10)
p=0.0042
Percent survival
% Weight Change
Days Post Infection
C
EBOV Challenge (Guinea Pigs)
PBS
CA45 5mg
FVM04 5mg
CA45+FVM04 2.5+2.5 mg
CA45+FVM04 5+5 mg
mAb
% weight change
D
SUDV Challenge (Guinea Pigs)

Fig. 7

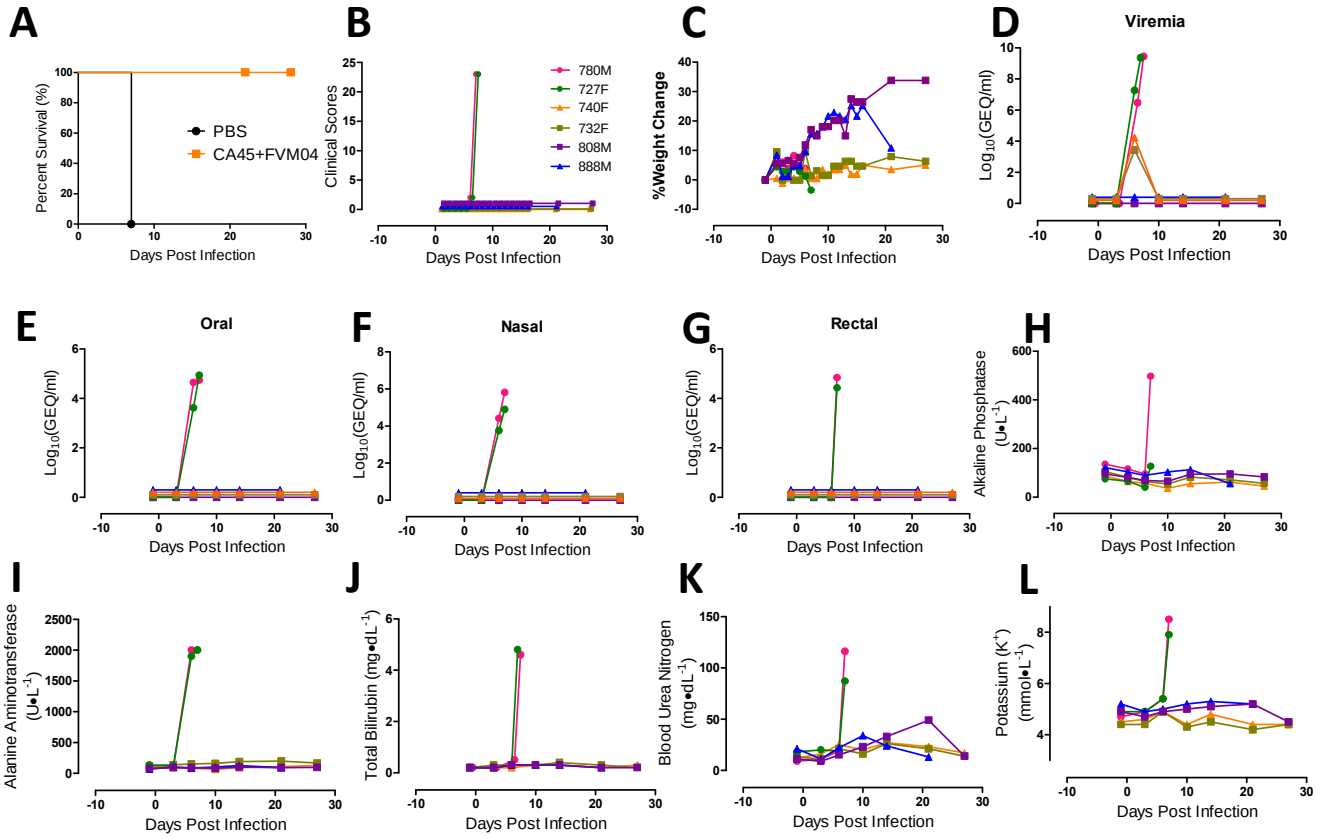
A
Percent Survival (%)
PBS
CA45+FVM04
Days Post Infection
B
Clinical Scores
780M
727F
740F
732F
808M
888M
Days Post Infection
C
%Weight Change
Days Post Infection
D
Viremia
Log10(GEQ/ml)
Days Post Infection
E
Oral
Log10(GEQ/ml)
Days Post Infection
F
Nasal
Log10(GEQ/ml)
Days Post Infection
G
Rectal
Log10(GEQ/ml)
Days Post Infection
H
Alkaline Phosphatase (U•L-1)
Days Post Infection
I
Alanine Aminotransferase (U•L-1)
Days Post Infection
J
Total Bilirubin (mg•dL-1)
Days Post Infection
K
Blood Urea Nitrogen (mg•dL-1)
Days Post Infection
L
Potassium (K+) (mmol•L-1)
Days Post Infection